THE MICROMETEOROID COMPLEX AND EVOLUTION OF THE LUNAR REGOLITH

F. HÖRZ, D. A. MORRISON, D. E. GAULT, V. R. OBERBECK,
W. L. QUAIDE AND J. F. VEDDER
210

A Preprint of a Manuscript from

THE PROCEEDINGS OF THE SOVIET-AMERICAN CONFERENCE ON THE COSMOCHEMISTRY OF THE MOON AND PLANETS

HELD IN MOSCOW, USSR, ON JUNE 4–8, 1974

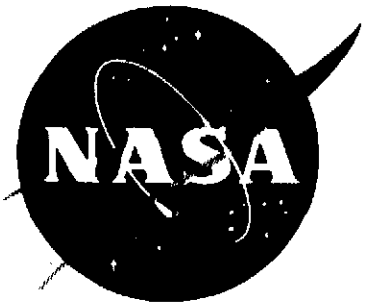

Distributed by

THE LUNAR SCIENCE INSTITUTE
HOUSTON, TEXAS 77058

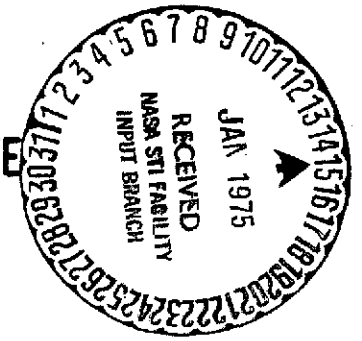

TO MAKE THE INFORMATION CONTAINED HEREIN AS WIDELY AND AS RAPIDLY AVAILABLE TO THE SCIENTIFIC COMMUNITY AS POSSIBLE. NASA EXPECTS TO PUBLISH THE ENGLISH-LANGUAGE VERSION OF THE PROCEEDINGS IN LATE 1975. THE FINAL TEXT MAY INCLUDE MINOR EDITORIAL CHANGES IN FORMAT, etc.

JOHN H. POMEROY, NASA HEADQUARTERS
TECHNICAL EDITOR

THE MICROMETEOROID COMPLEX AND EVOLUTION OF THE LUNAR REGOLITH

F. Hörz, D. A. Morrison
NASA Johnson Space Center
Houston, TX 77058, U.S.A.

D. E. Gault, V. R. Oberbeck, W. L. Quaide, J. F. Vedder
NASA Ames Research Center
Moffett Field, CA 94035, U.S.A.

D. E. Brownlee
University of Washington
Seattle, WA 98195, U.S.A.

and

J. B. Hartung
Max Plank Institut für Kernphysik
Heidelberg, Germany

Manuscript prepared for the Proceedings of "Soviet-American Conference on Cosmochemistry of the Moon and Planets", Moscow, June 4-9, 1974.

ABSTRACT:

Micrometeoroid Complex: The interaction of the micrometeoroid complex with the lunar surface is evidenced by numerous glass-lined microcraters on virtually every lunar surface exposed to space. Such craters range in size from <.1μm to approximately 2 cm diameter. Using small scale laboratory cratering experiments for "calibration", the observed crater-sized frequency distributions may be converted into micrometeoroid mass distributions. These "lunar" mass distributions are in essential agreement with satellite data for masses $>10^{-12}$g. However, for masses $<10^{-12}$ g there is considerable discrepancy. A radiation pressure cutoff does not exist because masses as small as 10^{-15} g can be observed. The absolute flux of micrometeoroids based on lunar rock analyses averaged over the past few 10^6 years is approximately an order of magnitude lower than presentday satellite fluxes; however, there is indication that the flux increased in the past 10^4 years to become compatible with the satellite data. Furthermore, there is detailed evidence that the micrometeoroid complex existed throughout geologic time.

Some physical properties of micrometeoroids may be deduced by comparing lunar crater geometries with those obtained in laboratory experiments. The proponderance of circular outlines of lunar microcraters necessitates equidimensional, if not spherical, micrometeoroids. Irregular shapes such as whiskers, needles, platelets, rods etc. - postulated in the past - do not contribute substantially to the micrometeoroid population and are rare, if not absent. The depth/diameter ratios of lunar microcraters are compatible with micrometeoroid-densities of 2-4 g/cm^3; densities <1 g/cm^3 can be excluded. These findings have astronomical significance with respect to comets, i.e., the source area for micrometeoroids.

Regolith-Dynamics: Monte Carlo based computer calculations as well as analytical approaches utilizing probabilastic arguments were applied to gain insight into the principal regolith impact processes and their resulting kinetics. Craters 10 to 1500 m in diameter are largely responsible for the overall growth of the regolith. As a consequence the regolith has to be envisioned as a complex sequence of discrete ejecta blankets. Such blankets constitute first order discontinuities in the evolving debris layer. The micrometeoroid complex then operates intensely on these fresh ejecta blankets and accomplishes some degree of mixing and homogenization. True mixing, however, can be accomplished only in an uppermost layer of approximatel 1 mm thickness,before a new ejecta event covers this layer and effectively removes it from the zone of active reworking. While, e.g., a 1 cm deep layer is turned over only one time in approximately 10^7 years, the uppermost 1 mm of that surface has been turned over already 250 times and the uppermost .1 mm more than 2000 times during the same time period. Therefore the lunar regolith becomes rapidly quiescent with depth. Though the micrometeoroid bombardment is extensive, a stratigraphic sequence may readily be preserved as evidenced in returned core tube materials. The erosion of lunar rocks caused by micrometeoroids is calculated at .3 to .6 mm per 10^6 years. The mean surface residence time of a rock of 1 kg in mass is in the order of 3×10^6 years, before it will be catastrophically destroyed by rupturing due to the impact of large micrometeoroids. This catastrophic destruction is far more effective than single particle abrasion in obliterating lunar rock specimen. Due to the vagarties of the random impact process, caution is necessary to delineate regolith dynamics from lunar sample analyses that are not based on a statistically significant number of observations.

Introduction:

With increasing resolution of lunar surface photographs prior to actual sample return it became more and more obvious that meteoroid impact had played a substantial role in the evolution of the lunar surface. It was discovered that meteoroid impact had operated on scales from 100's of km down to a few cm (Shoemaker et al., 1969). However, immediately upon cursory inspection of returned rocks it was learned that impact processes also occurred on still smaller scales: the ubiquitous presence of glass-lined lunar microcraters was ample evidence that virtually every lunar surface exposed to space was also subjected to the bombardment of micrometeoroids. In the meantime numerous laboratory investigations revealed that many properties of the lunar regolith are either directly or indirectly dominated by impact processes far beyond the original expectations. A proper understanding of many regolith processes therefore depends critically upon an understanding of the regolith impact history.

A thorough understanding of this history is only possible by combining lunar observational data, laboratory impact experiments and theoretical calculations. This report attempts to summarize such analyses. We will first discuss observational evidence of lunar microcraters and its implications to the micrometeoroid complex, including some astronomical consequences. We then will present some analytical and computer based calculations that will aid in the understanding of some principal regolith processes as well as their kinetics. Due to limited space some detailed argumentation cannot be presented and the reader must be referred to the original reports. In addition, a multitude of other interesting observations and interpretations had to be deleted, however, we attempted to present the most important aspects of the impact process as we understand them today.

I. LUNAR DATA OF THE MICROMETEOROID COMPLEX:

A) MICROCRATER-MORPHOLOGY:

Glass surfaces are by far the most suitable materials to study micrometeoroid impacts, because in comparison with crystalline rocks and breccias, they are usually smooth and observational conditions are optimize (Fig. 1). Furthermore, glasses are also the best investigated materials in small-scale laboratory cratering simulations. Thus-unless specified-the detailed morphology data, crater size frequency distributions and associated flux considerations are derived from lunar glass surfaces only.

Microcraters on lunar glass surfaces may range in diameter from less than .1μm up to approximately 2 mm; on crystalline rocks craters as large as 20 mm pit diameter were observed. Crater morphology differs characteristically as a function of absolute crater diameter [Bloch et al., 1971; Hartung et al., 1972(a, b); Morrison et al., 1973]. Craters smaller than 1μm are cup-shaped, glass-lined depressions - termed "pit" - with a pronounced rim of molten target material (Fig. 2(a)). Craters between 1 and 10μm pit diameter (Figs. 2(b), 2(c)) are transitional between the above morphology and that typical for craters larger than 10μm. Above 10μm diameter, they not only possess a central glass-lined pit but also a concentric spall zone (Fig. 2(d)). The spall zone may or may not be totally spalled off for craters between 10μm and 50μm but all craters above 50μm diameters have a completely developed spall zone. Morrison et al. (1973) delineated the following relationship: $D_S = 2.37 \times D_p^{1.07}$, where D_S is the spall zone and D_p the pit diameter.

For comparison, identical structures produced in the laboratory are illustrated in Figs. 2(e) and 1(f). Laboratory crater studies performed by electrostatic particle accelerators (Vedder, 1971, 1972; Fechtig et al., 1974; Mandeville and Vedder, 1971; Neukum, 1971; Schneider, 1972; Vedder and Mandeville, 1974; Mandeville, 1972), indicate that a glass-lined pit is only produced at projectile velocities exceeding 3 km/sec. The development and extent of a spall zone characteristic for the larger lunar craters requires velocities in excess of 5 km/sec.

B) PHYSICAL PROPERTIES OF MICROMETEOROIDS:

Laboratory simulations by Mandeville and Vedder (1971); Kerridge and Vedder (1972); Vedder and Mandeville (1974) and Mandeville (1973) have demonstrated that the outline of the central pit crater is controlled by projectile shape and angle of incidence and that the crater depth is dependent on projectile density and impact velocity.

Brownlee et al. (1973) measured crater-circularities from Scanning Electro Microscope (SEM) photographs that were taken with the electron-optical axis nor to the cratered surface. A "circularity index" was defined as the ratio A_m/A_c, where A_m is the area measured along the inferred intersection of the surrounding target surface with the inside of the pit rim, while A_c is the area of the smallest circle which just encloses A_m. Circularity indices measured for 131 micron sized craters demonstrate the rarity of highly noncircular pits (Fig. 3). Many of the noncircular craters in Fig. 3 are elongated and shallow indicating that they were produced by oblique impact rather than highly irregular projectiles (Brownlee et al., 1973, Hörz et al., 1974). By comparison with laboratory simulations using

irregular projectiles (Kerridge and Vedder, 1972), it is concluded that highly nonspherical shapes such as rods or platelets are rare or non-existant in the micrometeoroid complex. If dust grains were modeled as prolate ellipsoids then the observed crater circularities suggest an average length to width ratio of <2.

Depth/diameter ratios were determined for 70 craters (Brownlee et al., 1973) using the contamination line profiling technique of Vedder and Lem (1972) and parallax measurements from SEM stereo photos. The crater depth/diameter ratios refer to the maximum pit-depth below the original uncratered surface divided by the mean diameter of the inside of the pit rim. Figure 4 illustrates the results of 70 lunar craters in histogram form together with laboratory cratering data of Vedder and Mandeville (1974). Because the laboratory data does not extend beyond 13 km/sec impact velocity and because the velocity distribution of small meteoroids is not well known, it is not possible to determine exact particle densities. It is obvious, however, that the data are entirely inconsistent with micrometeoroid densities less than unity. The rarity of deep craters also appears to exclude the possibility that a significant fraction of particles could have densities as high as iron. Figure 4 apparently implies that most micrometeoroids (<50μm diameter) have densities in the 2-4 g/cm^3 range, if one assumes an average impact velocity of 20 km/sec. Even for velocities between 10 and 30 km/sec, the above densities are approximately valid.

Only ≈10% of the total crater population may offer different interpretations. Of those exceptions, the so-called "pitless" craters are by far the most abundant (≈80%). They do not possess a glass-lined pit (Fig. 5(a)) and could be interpreted as low velocity, "secondary" craters. However, as illustrated in Fig. 5(b) and as observed numerous times, there is strong evidence that many "pitless" craters did indeed have a glass-lined pit, which was spalled off either during crater formation or thereafter (McKay and Carter, 1972). Thus, many of these structures are also potential candidates for a "primary" origin (Hartung and Hörz, 1972). Another exceptional crater-type, termed "multiple pit crater," is illustrated in Fig. 5(c); Fig. 5(d) documents a laboratory equivalent produced by an agglutinate of minute glass spheres (Vedder and Mandeville, 1974). Consequently it is conceivable that "multiple pit craters" are indeed caused by projectiles of low density and nonhomogeneous mass-distribution, i.e., "aggregate" structure; however, they are rare exceptions and far less frequent than suggested by Verniani (1969), Hughes (1973) and many others.

C) CRATER POPULATIONS ON LUNAR ROCKS:

In analogy to large scale lunar surfaces (Gault, 1970; Shoemaker et al., 1969; and others), two basic types of crater populations need to be distinguished: a) "production" - and b) "equilibrium" populations. By definition, "production populations" are limited to rock surfaces of low, absolute crater densities, i.e., of short exposure periods. With time, more and more impacts will occur in already cratered areas until

finally the surface becomes so densely cratered that each new event will destroy an already existing one. Such a surface has reached "equilibrium". "Transition populations" are intermediate between "production" - and "equilibrium" conditions. Most lunar rocks are either in transition or equilibrium condition; genuine production populations are rare.

Because production surfaces exclusively display a complete record of all craters produced, only they are suitable to deduce mass-frequencies and the flux of micrometeoroids.

Cumulative crater size distributions for production populations on samples 12054 (Hartung et al., 1972(b)) and 60015 (Neukum et al., 1973) are shown in Fig. 6; though other genuine production populations were investigated the two curves illustrated are considered the best available over the size range indicated. The absolute crater densities for the two samples differ by almost a factor of 2, reflecting different times and/or geometry of exposure. The relative crater size frequency, however, is nearly identical.

Figure 7 illustrates "production" data resulting from SEM studies. The relative frequencies were normalized to surface 15205 at a pit diameter of 1μm. The illustrated data are considered the best available. The differences in the distributions and the presence of an inflection at pit-diameters between 1 and 10μm are subject to a variety of interpretations. They will be discussed later.

Because the rock surfaces that have reached "transition" and/or "equilibrium" conditions are less suitable to study the micrometeoroid complex, they will not be treated extensively here (Hörz et al., 1971;

Morrison et al., 1972; Neukum et al., 1973; Hartung et al., 1973; Schneider and Hörz, 1974). However - if coupled with solar flare track exposure ages - they may still contribute to the flux determination of micrometeoroids; minimum fluxes may be obtained, because a number of the craters produced are destroyed and not observable anymore.

D) MASS-FREQUENCY OF MICROMETEOROIDS:

Crater simulation experiments provide the only basis to obtain information concerning the mass distribution of micrometeoroids by converting crater dimensions into projectile parameters. The physical processes governing impact cratering are complex and presently not understood in great detail, despite considerable laboratory work. Especially, the energy partitioning for small and large scale cratering and the effects of target strength, gravitational forces and varying impact velocities, i.e., appropriate "scaling laws," are still subject to experimental work that ultimately will result in a theoretical understanding. Therefore, extrapolations from laboratory data may allow a variety of empirical calibration approaches.

Four basic calibration techniques for microcraters are currently in use (Fig. 8). Two are based on electrostatic dust accelerator experiments (Mandeville and Vedder, 1971; Vedder, 1971; Neukum et al., 1972; Schneider et al., 1973), and two calibration techniques utilize results from ballistic ranges (Moore et al., 1965; Gault, 1973) while Nagel (1973) employed a lithium plasma gun (for more detailed discussion see Hörz et al., 1974).

Relative crater size frequency distributions ranging from .1 to almost 1000 microns pit diameter may be constructed from the data presented in Figs. 6 and 7 by normalizing the absolute crater densities with respect to exposure time, exposure geometry and surface area. An important assumption underlying such a normalization is that these relative frequencies remained constant with time, because surfaces of different crater densities, i.e., different absolute exposure times, need to be normalized. Fig. 9 shows such a normalized, differential crater-frequency distribution based on glass-surfaces 12054, 60015 and 15205. The corresponding mass- and energy-scales are based on the calibration by Gault (1973) as shown in Fig. 8. For masses $>10^{-10}$g (=impact energies above 200 ergs) this distribution is in basic agreement with that obtained by satellite- and ground-based measurements (Millmann, 1973; Dohnanyi, 1972). Though the irregularity of the distribution at lower masses will be more thoroughly discussed later, it can already be seen that:

1. Particles in the 10^{-15} to 10^{-13} g range are most numerous.
2. The bulk of the meteoroid mass or energy impacting the moon is confined to particles 10^{-8} to 10^{-3} g in mass (see also Gault et al., 1972; Hartung et al., 1972(b)).

E) FLUX OF MICROMETEOROIDS:

Micrometeoroid fluxes are obtained by correlating absolute crater densities with the absolute exposure age. A summary of such correlations for binocular crater counts on selected rocks is given in Table 1 and illustra in Fig. 10, using the cumulative crater frequency for pits above 500µm diamet

Most data points shown lie below possible correlation lines and therefore are in or approaching equilibrium with respect to cratering. A correlation line corresponding to a crater production rate of 5 pits with diameters equal to or greater than 500 microns per cm^2 per million years lies within a factor of 2 of data for 12054, 12017, 12038, and 14301. Upon visual inspection of these samples, only rock 12038 was not clearly in production with respect to cratering. A factor of 2 is the estimated uncertainty in the solar flare track method used for the exposure time measurements.

Another approach to measure the meteoroid flux and possible changes with time has been pursued by Hartung, et al., 1974. Separate solar flare track exposure ages were determined for 56 individual pit craters larger than 20μm on rock 15205. The results illustrated in Fig. 11 indicate that the formation ages of these craters are not uniformly distributed; significantly more craters are produced during the last 10,000 years. Thus it appears that the present-day micrometeoroid flux is enhanced over that of the past 10^4 to 10^5 years by slightly more than an order of magnitude. The values obtained for the past 3000 years are in good agreement with present-day satellite measurements (Gault et al., 1972; Dohnanyi, 1972).

II. DISCUSSION OF THE MICROMETEOROID COMPLEX:

A) IMPLICATIONS OF PHYSICAL PROPERTIES

Based on laboratory cratering experiments, the morphologies of microcraters are interpreted to indicate, that they were formed by equidimensional, nonporous projectiles of densities between 2 and 4 g/cm^3,

which impacted with velocities in excess of 5 km/sec. These results are in part contrary to popular hypotheses and they may have significant astronomical consequences.

A cometary origin for micrometeoroids is strongly suggested by a variety of independent analyses (e.g., Dohnanyi, 1972; Zook and Berg, 1974). The particulate matter within comets is believed to represent unfractionated, solar abundances similar to Type 1 carbonaceous (CI) chondrites. Our mass densities are entirely consistent with CI chondrites, the constituents of which range in density from approximately 1.5 gr/cm^3 for aggregates of phyllo-silicates to magnetite grains of density 5 gr/cm^3 (Jedwab, 1971).

Much lower densities with an average of .5 to .8 gr/cm^3 have been suggested for the somewhat larger meteors, i.e., particles $>10^{-6}$ g (Verniani, 1969; Hughes, 1973). Though our detailed analysis of crater morphologies is confined to craters below 100μm diameter, i.e., particles $<10^{-8}$ gr, even pit craters larger than 1 cm, caused by particles approximately 10^{-3} g, display qualitatively the same morphologies. Though precise laboratory calibrations are not available for such large structures, we suggest that most particles of 10^{-6} to 10^{-3} gr may also have a density of more than unity.

The equidimensional character of micrometeoroids may also have significant astronomical implications, if we accept a cometary source. Traditionally it is suggested that such materials are similar if not identical in chemistry and shape to grains found in carbonaceous chondrites, because they are believed to represent primordial condensates from similar environments in the solar nebula. These grains are thought to be vapor

growths products of highly nonspherical shape like platelets, rods and whiskers (Kerridge, 1964; Donn, 1964; Arrhenius and Alfvén, 1971; Kerridge and Vedder, 1972). Such grains were observed in a variety of carbonaceous meteorites, e.g., Allende, which is thought to be a fine example of "early condensates" (Grossman, 1972). Clearly the microcrater circularities are incompatible with such elongated grains. These findings either imply that the postulated grain shapes are incorrect and virtually non-existing in the environment of comet-formation or that the micrometeoroid complex is also the result of multiple collisional events prior (!) to incorporation into cometary matrices. Recent developments in meteorite research provided strong evidence that collisional processes in the early history of the solar system may have played a dominant role.

Regardless what caused the micrometeoroids' equidimensional if not spherical shape: needles, platelets, rods, whiskers and other elongated or irregular particles seem not to make up a significant part of cometary silicates, if one accepts at all a cometary source area. The possibility that most of these particles constitute debris of collisional processes during accretion rather than primary condensates cannot be excluded.

B) MASS-FREQUENCY:

The frequencies of micrometeoroid masses ranging from 10^{-15} to 10^{-3} g are summarized in Fig. 12, together with a variety of satellite- and earth-based measurements. Two types of microcrater frequencies are observed: That displayed by samples 15205, 15076 and 15017 and that of sample 15286. Though experimental conditions (most dominantly target-smoothness and total number of craters counted) may be responsible for

subtle differences of the first type, the different behavior of 15286 seems beyond statistical error. Rock 15205 is based on 950 craters and sample 15286 on 500 craters. Thus, two questions remain: (1) Why are there two different frequency types? and (2) What causes an apparent bimodal mass distribution?

Sample 15286 is unique, though there are other samples (e.g., 12024,81 and 14257,F; Neukum et al., 1972) that may be similar. Their different mass-frequencies may be caused by extreme solid angles of exposure (Neukum et al., 1973) that effectively influence the energy-distribution, because of the increased effects of oblique impact (Gault, 1973). It is also conceivable that such surfaces were essentially pointing towards lunar North, i.e., out of the ecliptic plane, where they potentially could intercept a different population of cosmic dust than within the ecliptic plane.

Curves 15205, 15076 and 15017 are believed to be typical for micrometeoroids impacting the moon, simply because such distributions are the most frequent ones. Samples 60502,17; 15927,3; 15301,79 (Schneider et al., 1973) and 15015 (Morrison et al., 1973) yield similar results. The cause of this apparent bimodal mass-distribution is presently unknown. However, it is conceivable that the larger masses represent the cometary particle population that is spiraling towards the sun. During and upon solar approach, individual particles may suffer fragmentation as well as melting and/or vaporization; both processes would result in numerous particles of very small sizes. Upon close solar approach they may be propelled away from the sun again by solar radiation and have a second opportunity to encounter the lunar surface (Harwit, 1963; Zook and Berg, 1974).

Subtle differences in crater populations may yet be caused by a completely different mechanism. Morrison et al. (1973) and Blanford et al. (1974) report that lunar rock surfaces are significantly modified on the micron scale by the accretion of regolith-particles; most dominantly disk shaped, glassy splashes and droplets. These accretionary objects are so numerous that they accumulate obviously at a faster rate than the surface is destroyed by microcraters. Given sufficient time they may even build up layers of a few microns in thickness, giving some of the hand specimen a typical, patinated appearance. Thus a "constructive" accretion process is competing with the "destructive" cratering process and the micron size crater population may be somewhat modified. The unambiguous presence of particles below 10^{-15} g in mass, however, negates the existance of a radiation pressure cutoff. According to Gindilis et al. (1969), the lack of such a cutoff is highly compatible with particle densities of 2-4 gr/cm^3, i.e., with silicates, for which gravitational forces appear to dominate radiation pressure; this result corroborates our conclusions about particle densities.

Figure 12 also illustrates one fundamental advantage of lunar glass-surfaces as micrometeoroid detectors: At present, the lunar rock detector spans 12 orders of magnitude in mass and thus possesses a "dynamic range" duplicated nowhere. The potential identification of a bimodal size distribution is only due to such a large dynamic range.

Additional work with carefully selected samples is required to clarify what causes the two basic frequency types and the apparent bimodal

distributions. The above explanations have to remain tentative until carefully selected and precisely oriented surfaces are investigated in detail.

C. MICROMETEOROID FLUX:

A detailed comparison of micrometeoroid fluxes derived from lunar sample analyses and satellite measurements is presented in Fig. 13. It is impossible to discuss each detail and thus we offer a few general comments only quoting Hörz et al., 1974:

> "The moon is a rotating sampler, and the directional distribution of micrometeoroids is extremely non-uniform as shown by Berg and Grün (1973) and Hoffmann et al.(1973). Accordingly, the meteoroid flux differs about 3 orders of magnitude between the direction of the earth's apex and anti-apex. Furthermore, particles $>10^{-12}$ g are collected almost exclusively during the apex orientation of the Pioneer and HEOS sensors. Hence, in this mass range, also the moon may collect particles from only the apex direction. As a consequence, a "detector" on the rotating lunar surface can "register" meteoroid impacts effectively only part of the time. Therefore, fluxes derived from lunar crater statistics may have to be increased by as much as a factor of π for comparison with satellite data that were taken in the apex direction. Also, apex-pointing satellite data generally have been

corrected upward to a standard 2π-sterad exposure angle, assuming an isotropic flux. Thus, an actual anisotropy (as reported by the HEOS and Pioneer experiments) leads to an overestimation of the flux. Therefore, the satellite results seem to represent an upper limit for the flux.

"The "apex" particles show an average impact velocity of only 8 km/sec (Hoffmann et al., 1973). The fluxes from lunar rocks, however, are calculated with a standard velocity of 20 km/sec. The necessary corrections will increase the projectile masses and thereby effectively enhance the moon-based flux for masses $>10^{-10}$ g by a factor of approximately 5.

"The situation for masses $<10^{-12}$ g is highly complex. Berg and Grün (1973) have reported that most events of these masses occur with particles that have relative velocities of at least 50 km/sec. The lunar flux curves given for these masses in Fig. 12 are, however, based on a 20 km/sec impact velocity; if corrected to 50 km/sec, they will shift towards smaller masses, possibly as much as a factor of 10."

As a consequence the fluxes derived from lunar crater statistics may agree within the order of magnitude with direct satellite results if the above uncertainties in velocity and directional distribution are considered.

Fig. 14 presents some basic constraints derived from a variety of independent lunar studies on the flux of micrometeoroids and larger objects. The only direct measurements are the impact events registered by the Passive Seismic Experiment (Latham et al., 1973) and the micrometeoroids encountered by the spacecraft windows (Cour-Palais, 1974). Upper limits on the flux can be derived from the mare cratering rate (Shoemaker, 1971; Hartmann, 1972; Soderblom and Lebofsky, 1972). Accordingly, the flux over the past 3.0×10^9 years has remained fairly constant. The "geochemical" evidence is based on the abundance of siderophile trace elements indicative of type and amount of meteoritic contamination in the lunar soil (Anders et al., 1973). Erosion rates on lunar rocks range from approximately .2 to 2 mm/10^6 years (Barber et al., 1971; Rancitelli et al., 1973; Crozaz et al., 1972). Taking the highest erosion rate and applying cratering data of Gault (1973), an upper flux limit may be defined. Furthermore, the negative findings on the Surveyor III camera lens (Brownlee et al., 1971) and the perfect preservation of the foot pad print of Surveyor III (Jaffe, 1970) also define an upper limit. A lower limit results from the study of solar and galactic radiation tracks in lunar soils (Fleischer et al., 1974; Bhandari et al., 1972; Goswami and Lal, 1974). It is found that some cm thick layers of regolith have resided on the lunar surface essentially undisturbed for $\approx 1\text{-}2 \times 10^7$ years. Because the regolith is believed to be reworked by micrometeoroids only, the flux could not have been significantly lower than indicated; otherwise still older residence times for the soil-layers would be obtained. Strictly, only the passive seismometer, the Apollo windows and the mare craters yield a cumulative mass distribution. All

other parameters are either a bulk measure of meteoroid mass or energy; the corresponding "flux" was calculated using the differential mass-distribution obtained from lunar microcraters. Accordingly the corresponding arrows may be shifted anywhere along the line defining the "upper" and "lower" limits.

The data shown in Fig. 11 (Storzer and Hartung, 1974) suggest that the present flux is significantly higher than the average flux over the last 10^4 to 10^5 years (Hartung et al., 1974). Gault et al. (1972) and Morrison et al. (1972) were the first ones to indicate such a possibility because absolute lunar rock exposure ages, erosion rates and survival times of rocks appeared to be incompatible with computed values that were based on present-day meteorite fluxes derived from satellites. Neukum (1973) expanded on these interpretations and his "historic" and "prehistoric" fluxes are incorporated in Fig. 13. Because the annealing behavior for radiation tracks during long-term exposure in the lunar environment is not well known and because all potential errors-both in the age dating as well as crater-counting-enter these considerations, a "historic" and "prehistoric" flux can only be tentatively proposed at present. The data of Hartung et al., 1974 present the strongest evidence to date.

Although the magnitude of the flux may have varied over geological times, the mass frequency distribution appears to have remained fairly constant. Frequencies measured on surfaces that were constituents of the soil (15927, 15301, 15001 and 60502) most likely do reflect the meteoroid-bombardment that is older than that of most rocks. Their size-frequency distributions agree within the accuracy of measurement with "recent" crater populations.

Brownlee and Rajan (1974; Rajan et al., 1974) discovered microcraters that are identical to lunar craters on the surface of glassy spherules, disloged from the interior of the Kapoeta meteorite. This meteorite is a loosely consolidated microbreccia and a striking meteoritic analog to lunar soil breccias in many aspects. The formation age of Kapoeta is approximately 4×10^9 years (Rajan, pers. communication, 1974). Within the counting accuracy, the size frequency distribution of the Kapoeta microcraters is identical to lunar ones. Brownlee and Rajan furthermore dated one spherule via solar flare tracks and derived a micro-meteoroid flux that is within an order of magnitude of the present-day flux; because the track retention over 4×10^9 years in glassy materials is poorly known, however, this exposure age and the resulting micrometeoroid-flux has still larger uncertainties than young lunar glass surfaces. Blanford et al. (1974) report numerous microcraters on feldspars separated from the very bottom (soil-sample 15001) of the 240 cm long Apollo 15 drill core. The observed crater-size frequency distributions are essentially identical to those of rock sample 15205 and 15017 (see Fig. 12). Because this soil was deposited at its site of collection more than 400 m.y. ago (Russ et al., 1972) the observed crater populations must have formed prior to that time. Micro-meteoroid craters are also found in virtually every "soil-breccia" as well as genuine soil-samples, though their actual geological time period of exposure is not known at present (Schneider et al., 1973). Taking typical noble-gas exposure ages of lunar soils as statistically representative average values of the individual components, it may safely be concluded that

micrometeoroid bombardment was active throughout geological time. From the presently available microcrater-size frequency distributions it also may be concluded that the mass-frequency distribution of micrometeoroids has not changed significantly, if at all.

The studies on surfaces of old exposure ages demonstrate another unique characteristic of the "lunar rock micrometeoroid detector": it is principally possible to delineate the flux and potential variations thereof through geologic history. Such potential variations are of considerable interest for the formation of the solar system for a varity of reasons:

(a) The presence of a minimum micrometeoroid mass may be determined as a function of geologic time. This mass, in turn, may be used to calculate upper limits on the solar radiation pressure and thus to the luminosity of the sun. Brownlee and Rajan (1974) have attempted such calculations based on the minimum crater diameter observed on the Kapoeta materials and they concluded that the solar luminosity at $\approx 4 \times 10^9$ years was not higher than 1.7 times its present value.

(b) The main source of micrometeoroids has to be sought in short period comets. Significant variations in the flux of meteoroids may be related to short period comet "activities", i.e., to an uneven, possibly sporadic rate of comet encounters that are capable of putting micrometeoroids with bound orbits into the inner solar system. In addition to these relatively short term fluctuations (millions of years) it is also possible that the rate of comet injection into the inner solar system has undergone a long term secular change due to a general depletion of the comet inventory.

(c) Micrometeoroid detectors onboard Pioneer 8/9 have intercepted a non-negligible fraction of interplanetary particles that have hyperbolic orbits and thus are interpreted to be of interstellar origin (Berg and Grün, 1973). Thus lunar rocks offer a potential opportunity to study interstellar grains.

Most of the above possibilities, however, will require substantial amounts of work and are - at present - considered exciting challenges for future research. They are mentioned above only to stress the uniqueness and exciting potential of cratered lunar rock surfaces.

III. LUNAR REGOLITH-DYNAMICS:

The lunar regolith is a layer of fragmental debris of variable thickness that lies upon fractured bedrock. Photogeologic investigations and detailed analysis of returned lunar materials revealed that repetitive meteoroid bombardment has been responsible for the formation of this layer to such an extent that other geological processes may be excluded. Impact cratering controls the overall growth of regolith, the lateral and vertical redistribution of material, the downslope mass wasting, the mixing and degree of homogenisation of individual layers, the erosion of lunar rocks, the evolution of regolith grain sizes, the formation of impact melts, agglutinates and breccias, the migration of volatile elements, the admixture of meteoritic components and other parameters that make up the physical, chemical and petrographic characteristics of lunar "soils". As a consequency it appears appropriate to combine observational lunar crater data and

experimental impact crater mechanics into computational models to arrive at a theoretical understanding of these processes.

A variety of computational results concerning mass-movement, erosion rate of rocks, etc., are available (Shoemaker, 1971; Gault et al., 1972; Ashworth and McDonell, 1973; Neukum, 1973 and others). However, all these analyses suffer from the fact that they yielded only "average" values because the computations did not account for the vagarities of the random impact process. Models that do however, account for the randomness of the impact process both in space and time have been developed recently and are described below. The models may be used to gain a qualitative if not quantitative insight in some of the above processes. Some of these models consider craters up to 1500 m in diameter and thus are of drastically different dimensions than the craters treated in the preceding sections. Furthermore it is also important to note that the models are principally independent of the absolute flux of meteoroids. The time parameter is linearly related to the total number of craters produced. Thus model elapsed times can easily be converted into absolute times by applying the best estimate of the absolute meteoroid and micrometeoroid infall rates.

A) LARGE SCALE REGOLITH CRATERING:

The gross-accumulation of the regolith debris layer has been the subject of a variety of treatments, e.g., Marcus (1966) and Shoemaker (1971). It has been demonstrated that the overall regolith thickness increases with increasing numbers of craters that range roughly in diameter from 10 to 1000 m. Oberbeck and Quaide (1968) pointed out that the growing debris

layer acts as a buffering medium and thus strongly controls the geometry of different crater sizes. Accordingly the actual thickness for a given lunar surface area can be related to the total number of craters produced as well as to the relative frequencies of differently shaped craters such as "normal", "flat-bottomed", "concentric", and "central mound" craters.

Oberbeck et al. (1973) have developed a large scale Monte Carlo based computer program that simulates the evolution of the regolith and that also predicts the relative frequencies of the above four basic crater morphologies for any given regolith thickness. It is important to note that these calculations were performed with observed, lunar cratering parameters, i.e., detailed crater geometries and distributions of associated ejecta blankets. No cratering scaling laws needed to be assumed.

A crater production size frequency distribution of $N = KD^{-3.4}$ was empirically determined and used throughout these calculations (N = cumulative number of craters larger than diameter D, i.e., >1 m). Some pertinent results are discussed below; for detailed information the reader is referred to Oberbeck et al., 1973.

Fig. 15 illustrates the relationship of the calculated median regolith thickness (R_m) as a function of absolute numbers of craters produced. A relationship of

$$R_m = 6.2 \times 10^{-5} K^{.64} \qquad (1)$$

is derived and may be used to predict the median thickness for any surface area where crater size-frequency distributions can be determined and where the cumulative crater production distribution has the form of $N = K \cdot D^{-3.4}$.

However, the regolith thickness is variable over distances measured in 100's of meters as evidenced by high resolution photography and field inspection by the astronauts, despite the fact that the overall reference surface must have been exposed to the meteoroid bombardment for the same period of time. Fig. 16 compares actually measured thickness distributions (Oberbeck and Quaide, 1968) with those obtained in the Monte Carlo simulations. The agreement is good and lends additional support to the hypothesis that the regolith at the sites investigated by Quaide and Oberbeck (1968) is primarily caused by impact comminution processes.

However, the above Monte Carlo model on regolith formation yielded additional information: With increasing thickness of regolith only larger and larger craters are capable to penetrate the existing, buffering debris layer. Thus, with increasing time, it takes larger and larger craters to excavate pristine bedrock. The Monte Carlo simulations therefore continuously monitored per each crater size class the totall volume excavated from the pristine substrate (V_s) and the already existing regolith layer (V_R) throughout the time required to build up the regolith to a given thickness. Fig. 17 illustrates the ratio V_s/V_R for three different regolith depths. The ratio V_s/V_R is a function of crater diameter and is described by:

$$V_s/V_R = C \cdot D^n \qquad (2)$$

Where C is a constant for a given distribution of craters (n = 1-1.3); furthermore C can be related to K in the crater distribution expression $N = KD^{-3.4}$ by

$$C = 1.02 \times 10^6 K^{-1.06} \qquad (3)$$

and by substitution

$$V_s/V_R = 1.02 \times 10^{6}K^{-1.06}D^{n} \quad (4)$$

Thus, over the range of values of K characteristic for e.g., mare terrains, the effective size boundary between mixing and new debris producing craters becomes progressively larger. The average mixing zone therefore becomes deeper. Accordingly, older and thicker regolith deposits should be more thoroughly reworked than more youthful ones.

Fig. 18 illustrates the cumulative contributions of various sized craters that have built up a regolith layer of 4.7 m median thickness. It is obvious from Fig. 17 and 18 that relatively small craters (e.g., <10 m in diameter) have contributed significant amounts to the overall regolith, but it is also readily seen that these contributions occurred while the regolith was relatively thin, i.e., in the early stages of regolith formation. At present it is predominantly structures >100 m in diameter that control the overall regolith growth while the smaller structures are confined to reworking these materials. As a consequence, the regolith-thickness increases in general and in particular during its more recent history (i.e., the past $\approx 10^{9}$ years) due to the effects of relatively large cratering events that are capable of excavating pristine bedrock. This newly added material will always be delivered on top of the existing debris in discrete swaths of ejecta. The regolith therefore has to be envisioned as a complex sequence of numerous, overlapping ejecta blankets. These discrete blankets constitute some first order discontinuities and heterogenieties in the evolving regolith. We will demonstrate in the next chapter that it is principally possible to preserve parts of these

blankets despite heavy meteorite bombardment. Though there will be extensive mixing there will not be complete homogenization of the regolith.

B) SMALL SCALE REGOLITH CRATERING:

It is obvious from the preserved stratigraphy in returned core tube samples that reworking has not obliterated all stratification in the regolith. It is just as obvious, however, that every stratum that resided at the very lunar surface has been subjected to the meteoroid bombardment and the reworking process which - due to the mass-frequency distribution of interplanetary matter - does operate on a micron to meter scale. The extent to which a stratum survives thus must be a function of its original thickness and length of surface residence time before it is blanketed by ejecta of sufficient thickness to effectively remove it from the active zone of reworking. Absolute parameters for these variables principally vary with absolute time; i.e., the cumulative number of craters produced. The absolute number of craters that contributed to the history of returned samples must certainly be larger than the numbers presently observable in the respective sampling areas because these are in crater-saturation for craters <100 in diameter (Shoemaker, 1971; Gault, 1970). Thus the potential surface history of sampled materials can only be understood if a continuous bombardment history is assumed in computational models.

Because meteoritic impact is a random process, any given point on the lunar surface has a unique history as compared to any other given point. On the other hand the dominant role of meteoroid impact suggests that over extended periods of time any two areas of a given size will have

experienced similar histories that differ only in details to a greater or lesser degree. Thus computational analyses that yield "average" values may be useful in understanding the basic processes, however, they should only be applied with extreme caution to actual sample data because of the uniqueness of each individual sampling location. "Averages" are certainly a valid framework for returned sample interpretations, however, they should only be applied if sufficient statistical sample data are available. For any individual data point such averages cannot be applied and may lead to grossly erroneous results, because significant deviations from the "average" have to be expected from a random process.

Gault et al. (1974) have shown that the probability Pu of a given point on the lunar surface remaining undisturbed, i.e., lying outside a crater of apparent diameter D in a time interval t is given by:

$$P_u = \exp.\ (-\pi N t D^2/4) \qquad (5)$$

where N is the flux of the randomly distributed impacting bodies per unit time and area which produce craters of diameter D. The probability P_c of a given point having been affected, i.e., lying within exactly n craters of size D can be expressed as:

$$P_{c(n)} = P_u\ (\pi N t D^2/4)^n/_{n(!)} \qquad (6)$$

Equation 6 is the poisson probability function. Using the values given by Molina (1943) for a range of $n = 0 - 153$ and $(\pi N t D^2/4) = .001 - 100$ and calculating additional terms up to $n = 10^6$, Gault et al. (1974) calculated how many times a given surface area may be impacted. A micrometeoroid mass-distribution of the form $N = 1.45\ m^{0.47}$ was used for 10^{-13} to 10^{-7} g meteoroid mass (m) and $N = 9.14 \times 10^{-6}\ m^{1.213}$ for projectiles 10^{-7} to 10^{3} g.

Furthermore a standard impact velocity of 20 km/sec together with laboratory cratering data into unconsolidated materials (Gault, 1973) were applied in these calculations. The principal result is shown in Fig. 19.

Virtually identical results (Fig. 20) were obtained in a Monte Carlo based computer-simulation by Horz et al. (1974), that applied the crater size frequencies of Fig. 6 and a random number generator to determine impact coordinates and the magnitude of each cratering event. The curve labeled "1x" in Fig. 20 indicates how much surface area is affected at least 1x. Note that 50% of the test surface (=44 cm^2) is already cratered after 8300 craters, 152 to 22500 μm in spall diameter. It takes more than a factor of 10 additional craters to affect the remaining 50%. Though qualitatively not surprising, these absolute numbers were unexpected. Furthermore Fig. 20 e.g., illustrates that by the time 99% of the surface is cratered at least 1 x (99% probability), 92% of the surface is already cratered twice, 81% has suffered at least 3 impacts, 59% is cratered 4 times, etc. As 99.99% of the surface are cratered at least once, 88% will already be affected at least 5 times, etc.

An extension of the data illustrated in Fig. 20 is presented in Fig. 21 which is based on 10^6 craters (Hörz et al., 1974). Per each model-elapsed time it was determined how often a given fractional surface area was impacted. Note that when the entire area (=100%) is cratered at least one time, 50% has suffered already 12 impacts and 10% surface was cratered at least 17x. Or alternatively if it takes time 1 to affect 50% of a lunar surface, it will take 3.8 times longer to affect 90%, a factor of

6.6 longer to cover 99% and finally 19 times longer to crater 100% of the surface. The model times indicated in Figs. 19-21 will be used in identical fashion throughout this report. Unit time is defined as the time required to affect 50% of the surface area at least 1x.

Figs. 19-21 illustrate a fundamental characteristic of the impact process. While finite--though admittedly small--surface areas may remain unaffected for long time periods, other areas have already suffered repetitive bombardment. Consequently within any cratered terrain, small surface areas may be encountered that have dramatically different bombardment histories despite the fact that they were exposed to the same micrometeoroid environment for the same period of time.

We now turn to the mixing of the regolith. The above models are also a measure of how much kinetic energy is deposited randomly in space and time into a unit area of lunar surface. Therefore one can associate with that energy either a crater diameter (as above) or a corresponding crater depth. Gault et al. (1974) applied these concepts using the meteoroid mass distribution and the probability theory given above together with cratering mechanics of Gault (1973). The number of impacts per unit area (e.g., Fig. 21) were converted into "depth excavated" because each crater diameter may be associated with a given crater depth. Results of such calculations are illustrated in Fig. 22. The absolute timescale is based on the Gault et al. (1972) micrometeoroid flux, assumed to be constant over geological times. Though these absolute rates of regolith turnover are considered realistic for about the past 10^8 - 10^9 years, they are certainly not valid for periods $>10^9$ years. Gault et al. (1974) therefore also calculated the same data for a time variable flux; these data are shown in Fig. 23.

The principal result of Figs. 21 and 23 is of course the high turnover rate of the very regolith surface, e.g., Fig. 22: while it takes approximately 10^7 years to completely turn over an 8 mm deep zone at least once the uppermost mm of the very same area has been turned over already 25(!) times; or when 99% of an 8 mm deep layer is turned over at least once, 50% of the same surface will have already been turned over to 1.4 cm depth. As a consequence there exists a very thin surface zone, approximately 1 mm in thickness in which extreme mixing and homogenization of components occurs. However, the lunar regolith becomes relatively quiescent rather quickly with depth, e.g., even with a meteoroid flux that accounts for an increase in bombardment (Fig. 23) in early lunar history (=2-3.8 x 10^9 years), a 1 m thick layer is turned over only once with 99% confidence. This accounts for the observation of Russ et al., 1972, that a major section of the Apollo 15 deep drill core was residing completely undisturbed on the lunar surface for the past 500 m.y. We therefore conclude that due to the mass frequency distribution of interplanetary matter that is vastly dominated by relative small particles in the 10^{-8} to 10^{-4} g mass range, only an upper mm is thoroughly mixed. before an adjacent larger impact event covers the area and effectively removes the mixing layer from the active reworking zone. It is thus possible to preserve the observed small scale stratigraphy in the regolith.

However, though each surface layer undoubtedly has its peculair surface history, it is not correct to conclude that each layer was deposited at the eventual site of recovery by one discrete impact event. Gault et al. (1968) and Stoffler et al. (1974) demonstrated that the

ejecta blankets of experimental impact craters in layered quartzsand targets has part of the original target-stratigraphy preserved, though in reversed sequence, i.e., overturned. Similar observations are also made around large scale nuclear and chemical explosion craters as well as terrestrial impact craters. e.g., the 25 km diameter Ries-structure, Germany (Schneider, 1971). As a consequence, each regolith crater on the moon will preserve - though certainly in a somewhat degraded fashion - the original stratigraphic section. Therefore a variety of discrete layers may be excavated and redeposited at the site of recovery by a large, single impact regardless whether they had drastically different exposure histories before this last depositional episode.

Furthermore processes other than direct deposition of impact ejecta blankets may also cause an apparent layering in the recovered regolith cores. For example: small scale slumping on the walls of regolith craters may be a significant process. It can also be envisioned that soft soil breccias ejected by a larger event completely desintegrate upon landing at significant distances from the primary crater. Rocks that survived such a landing at the end of a ballistic trajectory are subject to micrometeoroid erosion and their erosion products may be foreign to the new environment, thus causing a local "heterogeniety" and therefore a "layer" in the regolith-stratigraphy. Virtually nothing is known about the lateral dimensions of the regolith "layers" and it is possible that their areal extend is rather limited. Beyond any doubt however, caution is necessary to postulate that each observed layer was last deposited by one discrete impact event; such interpretations may be grossly in error.

C) LUNAR ROCK EROSION

Studies of the grain size distribution of individual cratering experiments (Moore et al., 1964; Hörz, 1969) revealed that the ejecta of one given event are significantly more coarse grained than grain sizes reported from the lunar regolith (e.g., King et al., 1973; McKay et al., 1974). Thus larger regolith-components must be broken up, i.e., "eroded", by small scale cratering events. The visual inspection of lunar rocks both on lunar surface photographs as well as in the laboratory reveals that micrometeoroid impact causes erosion and eventual destruction of rock-specimen exposed to space. The micrometeoroid complex operates on two different scales and accordingly results in two significantly different effects, i.e., "single particle abrasion" and "catastrophic rupture" (Schoemaker, 1971; Gault et al., 1972; Ashworth and McDonell, 1973; Neukum, 1973 and others).

"Single particle abrasion" is caused by relatively small craters compared to the overall size of a specific rock and it results in an effect similar to sandblasting. It is largely responsible for gradual mass wasting associated with a general rounding of the rocks (Fig. 24). In contrast, "catastrophic rupture" is accomplished only by craters of relatively large size with respect to a given rock mass, i.e., only by impacts of sufficient energy capable to generate penetrative fracture systems (Fig. 25).

Hörz et al. (1974) simulated the "simple particle abrasion" process via Monte Carlo based computer models; up to 10^6 craters 152 to 25000 μm in spall diameter were produced on a 25 cm^2 surface area. Fig. 26 displays

some computer generated profiles after a variety of crater numbers produced. Fig. 27 illustrates the average erosion depth as a function of time. Note the influence of a few, though big events in particular in Fig. 27, but also in Fig. 26. Applying a best estimate for the absolute micrometeoroid flux averaged over the past 10^6 years, Hörz et al. (1974) arrive at erosion rates for crystalline lunar rocks of .3 - .6 mm per 10^6 years. The erosion rate for breccias may be higher, because of less compressive target strength (Gault et al., 1972).

An additional result of the above Monte Carlo simulation relating to the "representative" nature of finite size rock chips available in the laboratory to delineate lunar surface processes is illustrated in Fig. 28. The computer iterated over the entire test surface and searched for the least (=shallowest) and most eroded (=deepest) "unit areas" that were defined as 5, 2, 1, .64 and .16 cm^2. The "extremes" in erosional state are compared to the average of the entire area in Fig. 27. The deviation from the average is a direct measure how typical or atypical small lunar rock chips may be with respect to their parent rock. The deviations observed are considerable and constitute ample evidence that the random nature of the impact process has to be seriously considered in the analysis of discrete, finite size rock ships. Unless it is demonstrated otherwise that such a sample is truly "representative" of the parent rock, the results obtained may only be used with caution to delineate "averages", e.g., solar flare particle track densities to determine the absolute expsoure age.

Gault et al. (1972) treated the destruction of lunar rocks due to "catastrophic rupture". The catasrophic breakup of rocks may be accomplished either by a single impact event of sufficient energy or by the cumulative effects of a number of smaller impacts; the rupture energy (E_R) is cumulative (Gault and Wedekind, 1970). The energy required to rupture a rock ($\cong$spherical body) of radius r can be described as:

$$E_R = 2.5 \times 10^6 \, S_c \, r^{-0.225} \qquad (7)$$

where S_c is the unconfined compressive strength of the rock in kilobars; E_R is the unit energy required per gram, rather than total mass, of a rock of radius r. It thus follows that relatively less energy is required to destroy a larger and larger rock specimen. Fig. 29 compares actual measurements of the very largest pit craters observed on lunar rocks and the relations expressed by equation (7). The agreement is good (Hartung et al., 1973.)Fig. 29 illustrates the mean survival time before catastrophic rupture occurs for various hypothetical rock material considering compressive strength and rock mass as the main variables (Gault et al., 1972).

Combining the results of "single particle abrasion" and "catastrophic breakup" the following conclusions emerge: while e.g., a 1 kg rock will survive catastrophic desintegration for about 3×10^6 years, it has suffered in the meantime "single particle abrasion" that effectively removed a surface layer of only about 1-2 mm thickness. Thus "catastrophic rupture" must be considered the vastly superior process in obliterating lunar rocks; single particle abrasion plays a minor role only, however it is still an order of magnitude more effective than sputtering processes caused by high energetic radiation (Ashworth and McDonell, 1974).

IV. CONCLUSIONS:

It was hopefully demonstrated that the study of lunar microcraters has significantly contributed to our present understanding of the micrometeoroid complex:

1) Contrary to popular astronomical hypotheses, the micrometeoroids have densities of 2-4 g/cm^3. They are also equant if not spherical in shape; forms like needles, whiskers, platelets, rods, etc. may safely be excluded.

2) The mass-frequencies from 10^{-12} to 10^{-3} g are in agreement with previous meteoroid data. However particle masses as small as 10^{-15} g are responsible for the formation of microcraters <.1 μm in diameter. This result negates the existance for the celebrated "radiation pressure cut-off" at particle masses $<10^{-12}$ g.

3) The average micrometeoroid flux for the past 10^6 years could be established within a factor of 5. In agreement with satellite measurements it is likely that the present micrometeoroid activity is about an order of magnitude higher than this long term average.

4) Though absolute flux data do not exist at the moment, there is ample evidence that the micrometeoroid complex existed throughout geological time.

5) The potential of the "lunar micrometeoroid detector" is not fully exhausted at the moment.

The micrometeoroid complex as well as larger meteoroids are primarily responsible for the evolution and physical-chemical makeup of the lunar regolith; they effectively control the overall regolith growth as well as small scale stratigraphy. The regolith has to be envisioned as a complex sequence of ejecta blankets that have not necessarily lost their integrity. The mixing, "gardening" and homogenization is largely confined to the uppermost layer of approximately 1 mm thickness. Lunar rocks are effectively destroyed by micrometeoroids with the "catastrophic rupture" process dominating the "single particle abrasion". These results will not only aid in the interpretation of lunar materials but other planetary surfaces as well.

REFERENCES:

Alexander, W. M., C. W. McCracken and J. L. Bohn (1965), Zodiacal Dust: Measurements by Mariner IV, Science, 149, 1240-1241.

Alexander, W. M., C. W. Arthur and J. L. Bohn (1971), Lunar Explorer 35 and OGO 3: Dust particle measurement in selenocentric and cislunar space from 1967 to 1969, Space Research, XI, 279-285 Akademie Verlag, Berlin.

Anders, E., R. Ganapathy, U. Krähenbühl and J. W. Morgan (1973) Meteoritic Material on the Moon, The Moon, 8, 1-24.

Arrhenius, G. and H. Alfvén (1971) Asteroidal theories and experiments, In: Physical Studies of Minor Planets, Proc. 12th Coll. Int. Astr. Union, Tucson, Ariz., pp. 213-233.

Ashworth, D. G. and J. A. M. McDonell (1973) Updated Micrometeorite Influx Rates on the Lunar Surface Deduced from New Measurements of the Solar Wind Sputter Rate and Surface Crater Statistics, COSPAR, Konstanz, Germany, May 23 - June 5, 1973, to appear in Space Research.

Barber, D. J., R. Cowsik, I. D. Hutcheon, P. B. Price and P. S. Rajan (1971) Solar flares, the lunar surface and gas-rich meteorites, Proc. Second Lunar Sci. Conf., Geochim. Cosmochim. Acta, Suppl. 2, v. 3, 2705-2714. MIT Press.

Berg, O. and E. Grün (1973) Evidence of Hyperbolic Cosmic Dust Particles, Space Research, XIII, Akademie Verlag, Berlin, in print.

Bhandari N., J. N. Goswami, S. K. Gupta, D. Lal, A. S. Tamhane and V. S. Venkatavaradan (1972) Collision controlled radiation history of the lunar regolith, Proc. Third Lunar Sci. Conf., Geochim. Cosmoshim. Acta, Suppl. 3, v. 3, 2811-2829. MIT Press.

Blanford, G., D. S. McKay and D. A. Morrison (1974) Accretionary particles and microcraters, Lunar Science V, 67-68, The Lunar Science Institute, Houston; also in Proceedings of Fifth Lunar Science Conference.

Bloch, M. R., H. Fechtig, W. Gentner, G. Neukum and E. Schneider (1971) Meteorite impact craters, crater simulations, and the meteoroid flux in the early solar system. Proc. Second Lunar Sci. Conf., Geochim. Cosmochim. Acta, Suppl. 2, v. 3, pp. 2639-2652, MIT Press.

Brownlee, D. E. and R. S. Rajan (1974) Micrometeorite craters discovered on chondrule like objects from Kapoeta meteorite, Science, 182, 1341-1344 (1973).

Brownlee, D. E., W. Bucher and P. Hodge (1971) Micrometeoroid flux from Surveyor glass surfaces, Proc. Sec. Lunar Sci. Conf., v. 3, 2781-2789, MIT Press.

Brownlee, D. E., F. Hörz, J. F. Vedder, D. E. Gault and J. B. Hartung (1973) Some physical properties of micrometeoroids, Proc. Fourth Lunar Sci. Conf., Geochim. Cosmochim. Acta, Suppl. 4, v. 3, pp. 3197-3212.

Cour-Palais, B. G. (1974) The flux of meteoroids at the Moon in the mass range 10^{-8} to 10^{-12} g from the Apollo window and Surveyor III TV camera results, Lunar Science V, pp. 138-140, The Lunar Science Institute, Houston.

Crozaz G., R. Drozd, C. M. Hohenberg, H. P. Hoyt, D. Ragan, R. M. Walker and D. Yuhas (1972) Solar flare and galactic cosmic ray studies of Apollo 14 and 15 samples. Proc. Third Lunar Sci. Conf. Geochim. Cosmochim. Acta, Suppl. 3, v. 3, 2917-2931. MIT Press.

Dohnanyi, J. S. (1972) Interplanetary objects in review: Statistics of their masses and dynamics, Icarus, 17, pp. 1-48.

Donn, B. (1964) The Origin and Nature of Solid Particles in Space, Ann. New York Academy of Sciences, 119, Art. 1, pp. 5-16.

Drozd, R. J., C. M. Hohenberg, C. J. Morgan and C. E. Ralston (1974) presented at Lunar Science "Geology Conference", Jan. 1974; to be published (Data on Exposure Age of Rock 68415).

Fechtig, H., J. B. Hartung, K. Nagel and G. Neukum (1974) Microcrater Studies, derived meteoroid fluxes and comparison with satellite borne experiments, Lunar Science V, pp. 222-224, The Lunar Sci. Institute, Houston, also in Proc. Fifth Lunar Science Conference.

Fleischer, R. L., H. R. Hart, Jr., G. M. Comstock and A. O. Evwaraye (1971) The particle track record of the Ocean of Storms. Proc. Second Lunar Sci. Conf. Geochim. Cosmochim. Acta, Suppl. 2, v. 3, 2559-2568. MIT Press.

Fleischer, R. L., H. R. Hart and W. R. Giard (1974) Surface history of lunar soils and soil columns, Geochim. Cosmochim. Acta, 38, 341-484.

Gault, D. E. (1970) Saturation and equilibrium conditions for impact cratering on the lunar surface: Criteria and implications, Radio Sci., 5, 273-291.

Gault, D. E. (1973) Displaced mass, depth, diameter and effects of oblique trajectories for impact craters formed in dense crystalline rocks. The Moon, 6, 32-44.

Gault, D. E. and J. A. Wedekind (1969) The destruction of tektites by micrometeoroid impact, J. Geophys. Res. 74, 6780-6794.

Gault, D. E., W. L. Quaide and V. R. Oberbeck (1968), Impact cratering mechanics and structures, in: Shock Metamorphism of Natural Materials, pp. 87-99, edited by B. M. French and N. M. Short, Mono-Book, Baltimore.

Gault, D. E., F. Hörz, and J. B. Hartung (1972) Effects of microcratering on the lunar surface. Proc. Third Lunar Sci. Conf., Geochim. Cosmochim. Acta, Suppl. 3, v. 3, 2713-2734. MIT Press.

Gault, D. E., F. Hörz, J. B. Hartung, and D. E. Brownlee (1974) Mixing of the lunar regolith, Lunar Science V, The Lunar Science Institute, pp. 260-262, also in Proceedings of the Fifth Lunar Science Conf.

Gindilis, L. M., N. B. Divari and L. V. Reznova (1969) Solar Radiation Pressure on Particles of Interplanetary Dust, Soviet Astronomy, A.J., 13, 114-119.

Goswami, J. N. and D. Lal (1974) Cosmic Ray Irradiation Pattern at the Apollo 17 Site: Implications to Regolith Dynamics, Lunar Science V, pp. 284-286, The Lunar Science Institute, Houston.

Grossman, L. (1972) Condensation in the primitive Solar Nebula, Geochim. Cosmochim. Acta, 36, 597-619.

Gürtler, C. A. and G. W. Grew (1971) The Lunar Orbiter Meteoroid Experiment, NASA TN-D-6266.

Hart, H. R., Jr., G. M. Comstock and R. L. Fleischer (1972) The particle track record of Fra Mauro, Proc. Third Lunar Sci. Conf., Geochim. Cosmochim. Acta, Suppl. 3, v. 3, 2831-2844. MIT Press.

Hartman, W. K. (1972) Paleocratering of the Moon, Review of Post-Apollo Data, Astr. Space Sci. 16, 183-199.

Hartung, J. B. and F. Hörz (1972) Microcraters on lunar rocks, Proc. 25th Int. Geol. Cong., Montreal, Section 15, Planetology, 48-56.

Hartung, J. B., F. Hörz and D. E. Gault (1972b) Lunar microcraters and interplanetary dust. Proc. Third Lunar Sci. Conf., Geochim. Cosmochim. Acta, Suppl. 3, v. 3, 2735-2753. MIT Press.

Hartung, J. B., F. Hörz and D. E. Gault (1972b) Lunar rocks as meteoroid detectors, In Proc. Internal Astron. Union Colloq., No. 13, The Evolutionary and Physical Problems of Meteoroids. In press.

Hartung, J. B., F. Hörz, K. F. Aitken, D. E. Gault and D. E. Brownlee (1973) The development of microcrater populations on lunar rocks, Proc. Fourth Lunar Sci. Conf., Geochim. Cosmochim. Acta, Suppl. 4, v. 3, 3213-3234.

Hartung, J. B., D. Storzer and F. Hörz (1974) Toward a lunar microcrater clock. Lunar Science V, 307-309, The Lunar Science Institute also in Proceedings of the Fifth Lunar Sci. Conf.

Harwit, M. (1963) Origins of the Zodiacal Dust Cloud, J. Geophys. Res. 68, 2171-2180.

Hawkins, G. S. (1963) Impacts on the Earth and Moon, Nature 197, No. 4869, p. 781

Hoffman, H. J., H. Fechtig, E. Grün and J. Kissel (1973) First results of the micrometeoroid experiment S 215 on the HEOS 2 satellite, COSPAR 1973, Konstanz, Germany, p. 114; in print: Space Research XIV.

Hörz, F. (1969) Structural and minerological evaluation of an experimentally produced impact crater in granite, Contr. Mineral. and Petrol. 21, 365-377.

Hörz, F., J. B. Hartung and D. E. Gault (1971) Micrometeorite craters on lunar rock surfaces, J. Geophys. Res. 76, 5770-5798.

Hörz, F., D. E. Brownlee, H. Fechtig, J. B. Hartung, D. A. Morrison G. Neukum, E. Schneider and J. F. Vedder (1974a) Lunar microcraters and their implications for the micrometeoroid complex, Planetary and Space Sciences, in press.

Hörz, F., E. Schneider and R. E. Hill (1974b) Micrometeoroid abrasion of lunar rocks: A Monte Carlo simulation, Proc. of the Fifth Lunar Science Conf., in print.

Hughes, D. W. (1973) Interplanetary dust and its influx to the earth's surface, COSPAR 73, Konstanz, Germany; in print: Space Research XIV.

Hutcheon, I. D., D. Macdougall, P. B. Price, F. Hörz, D. Morrison and E. Schneider (1974) Rock 72315; A new lunar standard for solar flare and micrometeorite exposure, Lunar Science V, The Lunar Science Institute, pp. 378-380.

Jaffee, L. D. (1970) Lunar Surface: Changes in 31 months and micrometeoroid flux, Science, 170, 1092-1094.

Jetwab, J. (1971) La Magnetite de le meteorite D'Orgueil, Vue au Microscope Electronique a Balayage, Icarus, 15, 319-340.

Kaiser, T. R. (1961) The determination of the incident flux of Radio-Meteors II: Sporadic Meteors; Monthly Notices Roy. Astron. Soc., 123, 265-271.

Kerridge, J. F. (1964) Low-temperature minerals from the fine-grained matrix of some carbonaceous meteorites, Ann. New York Academy of Sciences, 119, Art. 1, pp. 41-53.

Kerridge, J. F. and J. F. Vedder (1972) Accretionary Process in the Early Solar System: An Experimental Approach, Science, 177, 161-162.

King, E. A., J. C. Butler and M. F. Carman (1972) Chondrules in Apollo 14 samples and size analyses of Apollo 14 and 15 fines, Proceedings Third Lunar Science Conf., Geochim. Cosmochim. Acta, Suppl. 3, v. 1. pp. 673-686.

Konstantinov, B. P., M. M. Bredov, E. R. Mazets, V. N. Panov, R. L. Aptekar, S. V. Golenetskii, Y. A. Guryan and V. N. Jlinskii (1968) Micrometeoroid investigations on the satellite "Cosmos 135"; Cosmic Research, 6, 622-632.

Konstantinov, B. P., M. M. Bredov, E. R. Mazets, V. N. Panos, R. L. Aptekar, S. V. Golenetskii, Y. A. Guryan and V. N. Illinskii (1969) Micrometeors in circumterrestrial space observed by "Kosmos 163", Cosmic Research, 7, 817-821.

Lal, D. (1973) Hard rock cosmic ray archeology, Space Sci. Rev. 14, 3-102.

Latham, G., J. Dorman, F. Duennebier, M. Ewing, D. Lammlein and Y. Nakamura (1973) Moonquakes, meteoroids, and the state of the lunar interior, Proc. Fourth Lunar Sci. Conf., Geochim. Cosmochim. Acta, Suppl. 4, v. 3, pp. 2515-2527.

Lindblad, B. A. (1967) Luminosity functions of sporadic meteors and extrapolation of the influx rate to the micrometeorite region. Smithson. Contr. Astrophys., 11, 171-180 NASA SP-135.

Mandeville, J. C. (1972) Etude de crateres formes sur des surfaces de verre par l'impact de micrometeorides artificelles, Ph.D. Thesis, No. 1334, Toulouse, France; 97p. unpublished.

Mandeville, J. C. and J. F. Vedder (1971), Microcraters formed in glass by low density projectiles, Earth Planet. Sci. Letters, 11, 297-306.

Marcus, A. H. (1966) A stochastic model of the formation and survival of lunar craters, 2. Icarus 5, 165-177.

McKay, D. S., R. M. Fruland, G. Heiken (1974) Grain size distribution as an indicator of the maturity of lunar soils, Lunar Science V, p. 480-481, The Lunar Science Institute, Houston.

Millmann, P. (1973) The observational evidence for mass distribution in the meteoritic complex; The Moon, 8, 228

Molina, E. C. (1942) Poisson's exponential binominal limit, Van Norstrand, Princeton.

Moore, H. J., D. E. Gault and E. D. Heitowit (1964) Change of effective target strength with increasing size of hypervelocity impact craters, 7th Hypervelocity Impact Symposium, Tampa, Florida, Nov. 17-19, 1964.

Morrison, D. A., D. S. McKay and H. J. Moore (1973) Microcraters on Apollo 15 and 16 rocks. Proc. Fourth Lunar Sci. Conf., Geochim. Cosmochim. Acta. Suppl. 4, v. 3, 3235-3253.

Nagel, K. (1973) Experiments zur Kratersimulation. Master's Thesis, University of Heidelberg, Germany, unpublished.

Naumann, R. J., D. W. Jex and C. L. Johnson (1969) Calibration of Pegasus and Explorer XXIII Detector Panels, NASA TN, TRR-321.

Neukum, G. (1971) Untersuchungen über Einschlagskrater auf dem Mond. Doctor's thesis, University of Heidelberg.

Neukum, G. (1973) Micrometeoroid flux, microcrater population development and erosion rates on lunar rocks, and exposure ages of Apollo 16 rocks derived from crater statistics (abstract). In Lunar Science IV, pp. 558-560, The Lunar Science Institute, Houston.

Neukum, G., E. Schneider, A. Mehl, D. Storzer, G. A. Wagner, H. Fechtig and M. R. Bloch (1972) Lunar craters and exposure ages derived from crater statistics and solar flare tracks. Proc. Third Lunar Sci. Conf. Geochim. Cosmochim. Acta. Suppl. 3, v. 3, 2793-2810, MIT Press.

Neukum G., F. Hörz, D. A. Morrison and J. B. Hartung (1973) Crater population on lunar rocks, Proc. Fourth Lunar Sci. Conf., Geochim. Cosmochim. Acta. Suppl. 4, v. 3, 3255-3276.

Nilsson, C. S., F. W. Wright and D. Wilson (1969) Attempts to measure micrometeoroid flux on the OGO II and OGO IV satellites, J. Geophys. Res., 74, 5268-5276.

Oberbeck, V. R. and W. L. Quaide (1968) Genetic implications of lunar regolith thickness variations, Icarus, 9, 446-465.

Oberbeck, V. R., W. L. Quaide, M. Mahan and J. Paulson (1973) Monte Carlo calculations of lunar regolith thickness distribution. Icarus, v. 19, 87-107.

Rancitelli, L. A. (1973) Personal communication.

Rajan, R. S., D. E. Brownlee and F. Hörz (1974) The ancient micrometeorite flux, Lunar Science V, pp. 616-617, The Lunar Science Institute, Houston.

Russ, G. P., D. S. Burnett and G. J. Wasserberg (1972), Lunar Neutron stratigraphy, Earth Planet. Sci. Letters, 15, 172-186.

Schneider, E. (1972) Mikrokrater auf Mondgestein und deren Laborsimulation; Ph.D. Thesis, Heidelberg, Germany, unpublished.

Schneider, E. and F. Hörz (1974) Microcrater Populations on Apollo 17 Rocks, Icarus, in print.

Schneider E., D. Storzer, A. Mehl, J. B. Hartung, H. Fechtig and W. Gentner (1973) Microcraters on Apollo 15 and 16 samples and corresponding cosmic dust fluxes. Proc. Fourth Lunar Sci. Conf., Geochim. Cosmochim. Acta, Suppl. 4, v. 3, 3277-3290.

Schneider, W. (1971) Petrologische Untersuchungen der Bunten Breccie im Nördlinger Ries, N. Jb. Miner. Abh. 114, pp. 136-180.

Schonfeld, E. (1971) Personal communication (see LSPET (Lunar Sample Preliminary Examination Team)(1970)), Preliminary examination of the lunar samples from Apollo 12, Science, 167, 1325-1339.

Shoemaker, E. M. (1971) Origin of fragmental debris on the lunar surface and the history of bombardment of the moon, Instituto de Investigaciones Geologicas de la Diputacion Provincial, v. XXV, Universidad de Barcelona.

Shoemaker, E. M., R. M. Batson, H. E. Holt, E. C. Morris, J. J. Rennilson and E. A. Whitaker (1969), Observations of the lunar regolith and the earth from the television camera on Surveyor 7., J. Geophys. Res., 74, 6081-6119.

Soderblom, L. A. and L. A. Lebofsky (1972) Technique for Rapid Determination of Relative Ages of Lunar Areas from Orbital Photography, J. Geophys. Res. 77, 279-296.

Stöffler, D., M. R. Dence, M. Abadian, G. Graup (1974) Ejecta Formations and Preimpact Stratigraphy of Lunar and Terrestrial Craters: Possible Implications for the Ancient Lunar Crust, Lunar Science V, 746-748, The Lunar Science Institute, Houston.

Storzer, D. and J. B. Hartung (1974) in preparation

Vedder, J. F. (1971) Microcraters in glass and minderals, Earth Planet. Sci. Lett. 11, 291-296.

Vedder, J. F. (1972) Craters formed in mineral dust by hypervelocity microparticles, J. Geophys. Res., 77, 4304-4309.

Vedder, J. F. and H. Lem (1972) Profiling with the electron microscope, Photogrammetric Engr., 38, 243-244.

Vedder, J. F. and J. C. Mandeville (1974) Microcraters formed in glasses by projectiles of various densities, J. Geophys. Res. in print.

Verniani, F. (1969) Structure and Fragmentation of Meteoroids, Space Sci. Res. Rev. 10, 230-261.

Zook, H. and O. E. Berg (1974) A source for hyperbolic cosmic dust particles, Planetary and Space Sciences, in press.

FIGURE CAPTIONS:

Fig. 1. Large glass-coating on lunar rock 64455 with abundant microcraters. All structures are above 5 μm diameter and therefore display characteristic spall zones. Close to the fracture zone exposing the underlying anorthositic substrate, the crater densities are very high and approximate equilibrium. (Sidelength of picture: 3.2 cm.)

Fig. 2. Typical lunar and experimental microcraters on glass surfaces. Note the change of crater morphology with size:

(a) Very small lunar microcrater that displays neither concentric fractures nor a spall zone. Note the raised, glassy rim.

(b) Lunar crater that displays concentric fracture zone indicative of incipient spallation.

(c) Lunar crater with partially developed spall zone.

(d) Lunar crater with completely developed spall zone.

(e) Experimental crater (Al-projectile into soda lime glass; impact velocity: 9.9 km/sec).

(f) Experimental crater (Polystyrene projectile into soda lime glass; impact velocity: 5.7 km/sec; note shallow crater depth and compare to 1(a)-(e)).

Fig. 3. Histogram of the circularity index of 131 microcraters ranging in size from .2 to 80 μm diameter (rock 15286). Though not illustrated, the circularity index is independent of pit crater diameter.

Fig. 4. Experimentally determined depth/diameter ratios using projectiles with densities from 1 to 7 g/cm^3 and impact velocities from 3 to 13 km/sec. The inserted histogram on lunar depth/diameters is based on 70 craters.

Fig. 5. Unusual craters

(a) "Pitless" lunar crater. Note the similarities and possible transition to crater 5(b).

(b) Similar sized lunar crater with pit. Note that spallation action was severe enough to undercut the glass lined pit, leaving it barely attached to the crater bottom.

(c) "Multiple pit" crater on lunar glass-surface 15286.

(d) "Multiple pit" crater produced in the laboratory.

Fig. 6. Typical binocular crater size frequency distributions for lunar glass surfaces in production state (12054 is based on 960 craters; 60015 is based on 665 craters).

Fig. 7. Typical scanning electron microprobe crater size frequency distributions for small microcraters on lunar glass surfaces in production state (15205 is based on ≈1100, 15286 on ≈500 and 15017 on ≈300 craters).

Fig. 8. Various calibration methods presently in use to derive micrometeoroid masses from measured pit diameters (D_p) or spall-diameters (D_s). D_s/D_p is variable from rock to rock with values between 3.8 - 4.5 on lunar glasses. Note that agreement between various techniques is close, if a D_s/D_p of 4.5 is applied.

Fig. 9. Differential frequency of pit-diameters and their corresponding particle mass and energy distributions. The binocular data (12054, 60015) and SEM data (15205) are joined at a pit-diameter of 100 μm as indicated.

Fig. 10. Correlation of surface residence times of specific rocks mostly determined with solar flare tracks (see Table 1) and absolute frequency of pit-craters >500 μm in diameter/cm^2. A straight line going through the origin establishes the crater production rate, i.e., the flux of micrometeoroids >2 x 10^{-7} g. A best estimate for the average flux over the past 10^6 years is ≈5 pits/cm^2.

Fig. 11. Preliminary formation ages of 56 individual microcraters ranging in size from 20 to 300 micron pit diameter on glass surface 15205,51. Note the steep increase in crater production rate between 0 and 10^4 years, corresponding to a twofold increase every 3000 years.

Fig. 12. Comparison of the cumulative mass-frequency slopes of a variety of observational techniques, but in particular of five well documented lunar glass surfaces. Most individual satellite data do not give a differential flux; the position of the satellite data was constructed by extrapolating the slope from the cummulative mass-frequency curve of Dohnanyi (1972, Fig. 1). The length of the bars indicates the mass-range over which the corresponding slope is valid.

Fig. 13. Comparison of lunar and satellite micrometeoroid flux data.

Fig. 14. Constraints on the flux of micrometeoroids and larger objects according to a variety of independent lunar studies.

Fig. 15. The overall regolith growth as a function of craters produced, i.e., time (see equation 1).

Fig. 16. Empirically determined regolith thickness distribution for four different lunar surfaces measuring ≈200 km^2 each. The empirical determination is based on the abundance of various crater geometries reflecting the presence of a competent substrate. Note the good agreeemnt between observations and Monte Carlo cratering simulations.

Fig. 17. Relative contributions of pristine bedrock from the "substrate" for various crater sizes and regolith depths. The "volume regolith" is that volume that is reworked debris excavated by prior cratering. Note that predominantly the larger craters excavate bedrock and thus chiefly contribute to the overall regolith growth with increasing regolith thickness, i.e., time.

Fig. 18. Contributions (=volume%) of various source areas at depth "d" to the overall composition of a typical mare regolith having a median thickness of 4.7 m.

Fig. 19. Analytical model based on Poisson probability function describing how much surface area (%) will be affected by meteoroid impact how many times after given model elapsed times.

Fig. 20. Almost identical data as in Fig. 19 resulting from a Monte Carlo computer program. Note the multiple bombardment history of fractional surface areas with increasing time, i.e., 10^5 craters produced.

Fig. 21. General probability of multiple bombardment history for various fractional surface areas (total craters produced: 10^6; see text).

Fig. 22. The detailed turnover history of various regolith depths as a function of absolute time and a constant flux.

Fig. 23. Same as Fig. 22, however, using a meteoroid model flux that increases with geologic time to match the observed crater densities at the Apollo 12 landing site.

Fig. 24. Typical lunar rock (14310) illustrating the effects of single particle abrasion. As indicated by the soil line, parts of this rock were buried in the lunar regolith. The buried portion is characterized by sharp, angular fracture surfaces. In contrast, the surfaces exposed to the micrometeoroid bombardment are abraded and significnatly rounded.

Fig. 25. Lunar rock 73155 that has suffered an exceptionally large impact almost capable of catastrophically rupturing the entire hand specimen.

Fig. 26. Computer generated erosion profiles of a lunar rock. Per each number of total craters produced, profiles taken at 3 different localities (Y_{71}, Y_{76}, Y_{81}) are illustrated (white: volume eroded; stippled: remaining rock; the vertical exaggeration is 17x).

Fig. 27. Average erosion depth resulting from a Monte Carlo computer simulation. The best estimate for erosion is based on 10^6 craters, i.e., run 3. Notice the influence of some few, however very large craters.

Fig. 28. Extremes in deviation of erosional state of various, absolute surface areas (5, 2, 1., .64 and .16 cm^2) compared with the average of a 25 cm^2 surface.

Fig. 29. Spall and pit ciameters required for catastrophic rupture of a given rock mass based on experimental and observational results. D_p (destructive) is considered an upper limit for pit diameters observable on lunar rocks; D_c is an experimental limit referring to the crater diameter, i.e., spall diameter (D_s). D_s/D_p ratios in lunar rocks are typically 3.8 - 4.6. The agreement of observations on lunar rocks and experimental rupture is excellent.

Fig. 30. Calculated mean residence time before destruction by catastrophic rupture for spherical rocks of radius r and compressive strengths (S_c) that are exposed to the micrometeoroid bombardment. Masses of the largest particles ($M_{P_{max}}$) that are contributing to the rupture process are indicated.

NASA
S- 73- 22655

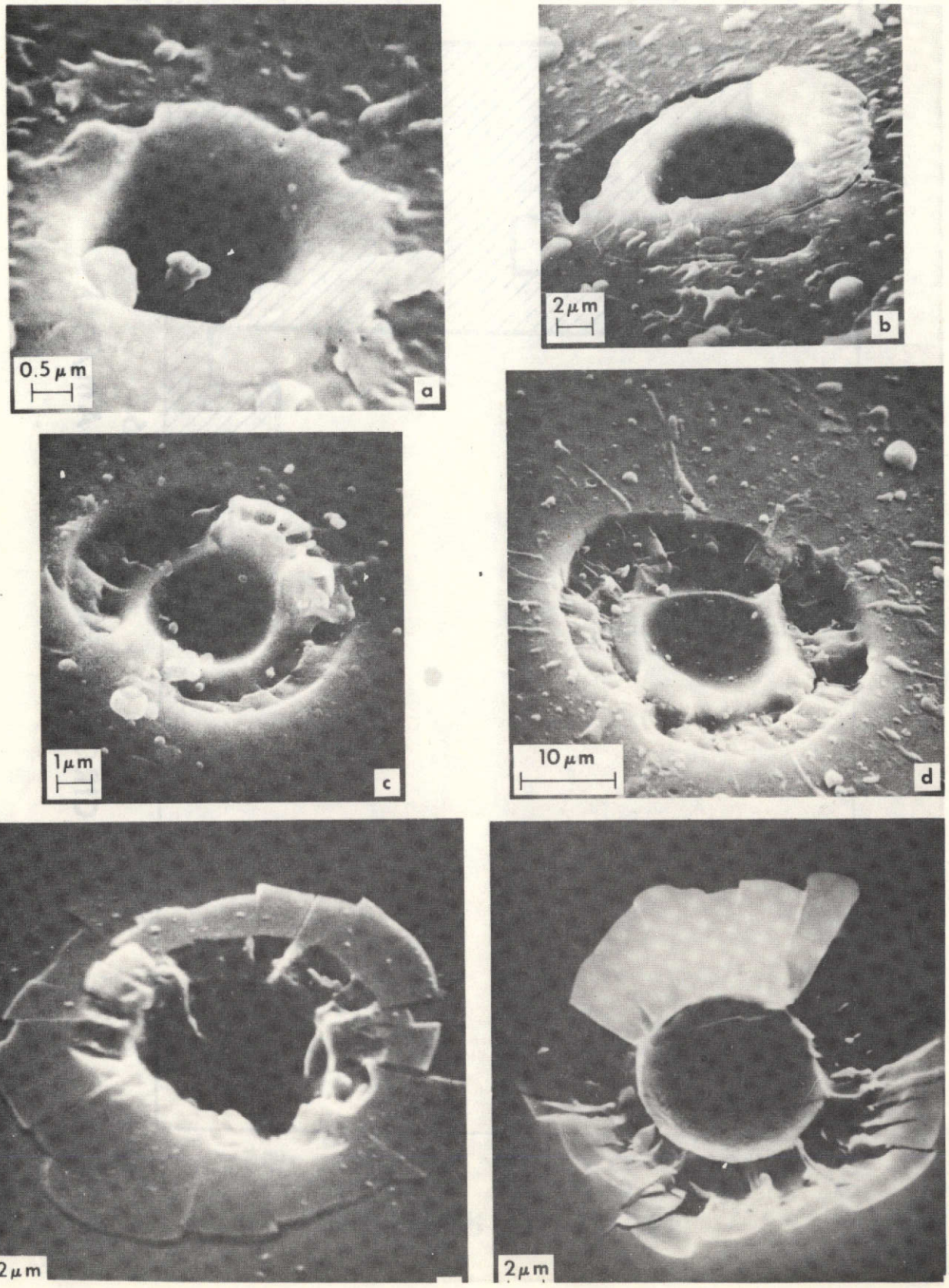

NASA
E- 73- 35689

Fig. 2

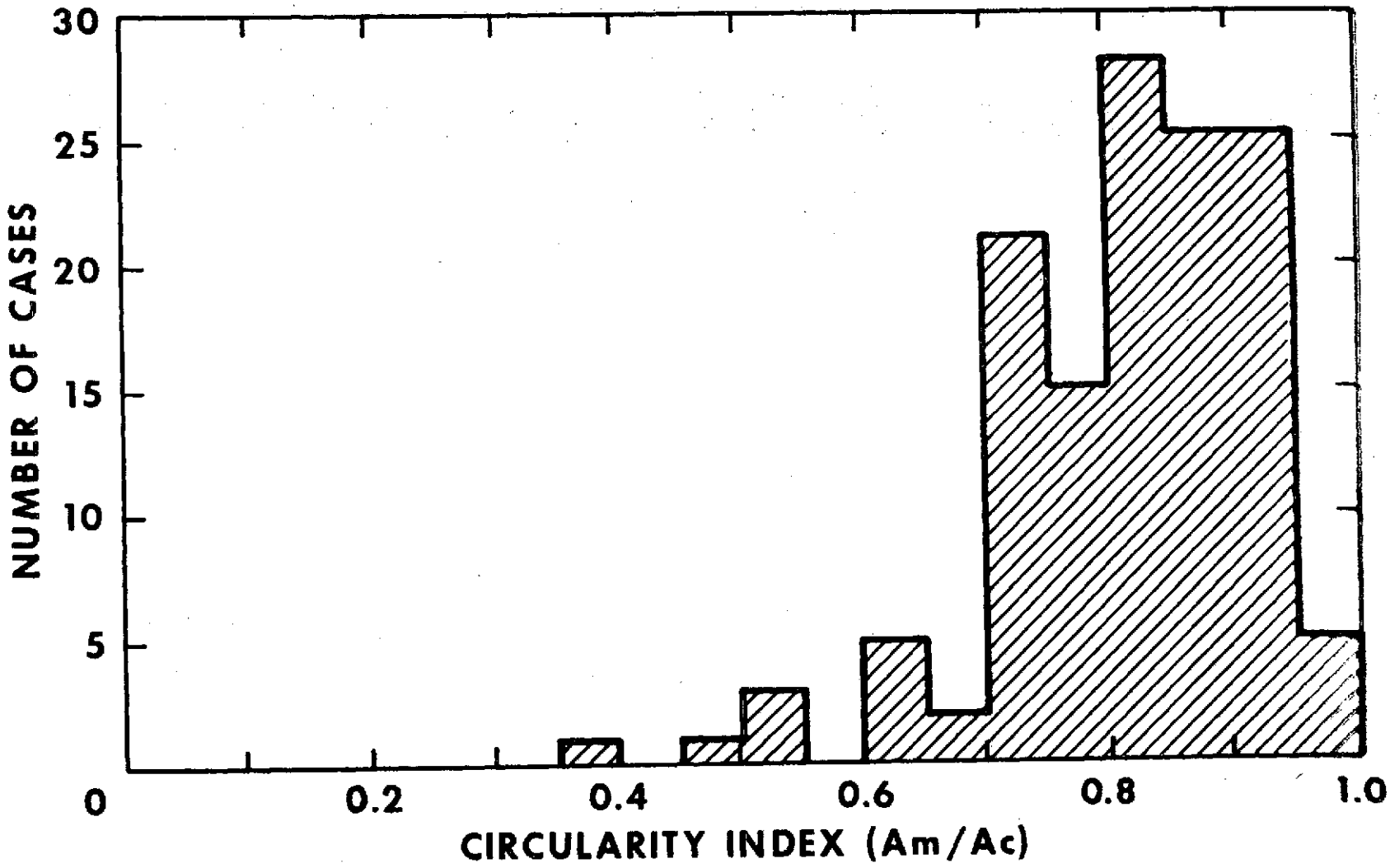
30
25
20
15
10
5
0
NUMBER OF CASES
0.2
0.4
0.6
0.8
1.0
CIRCULARITY INDEX (Am/Ac)

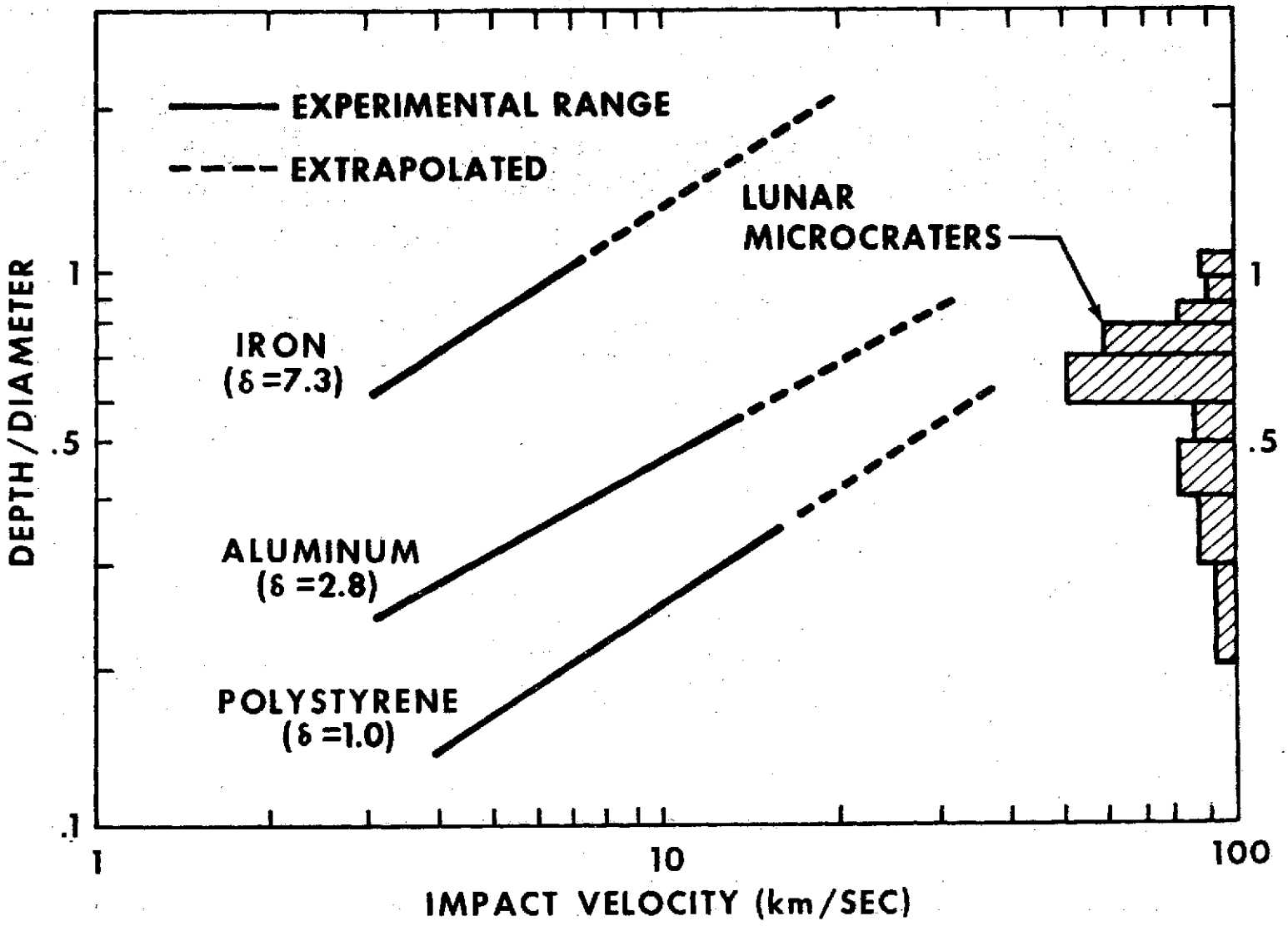
EXPERIMENTAL RANGE
EXTRAPOLATED
LUNAR MICROCRATERS
IRON (δ =7.3)
ALUMINUM (δ =2.8)
POLYSTYRENE (δ =1.0)
DEPTH/DIAMETER
1
.5
.1
1
10
100
IMPACT VELOCITY (km/SEC)

NASA
E- 73- 35888

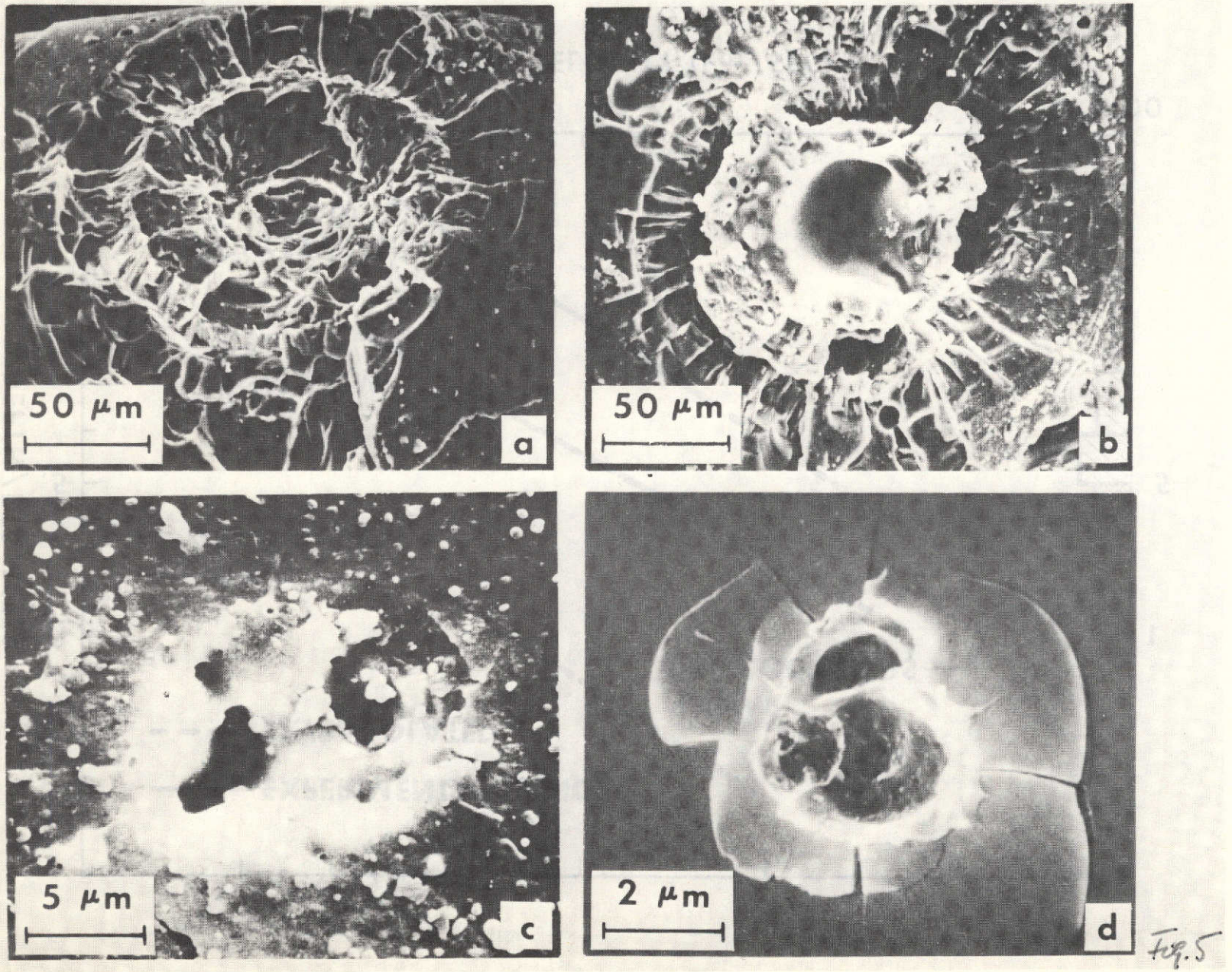

Fig. 5

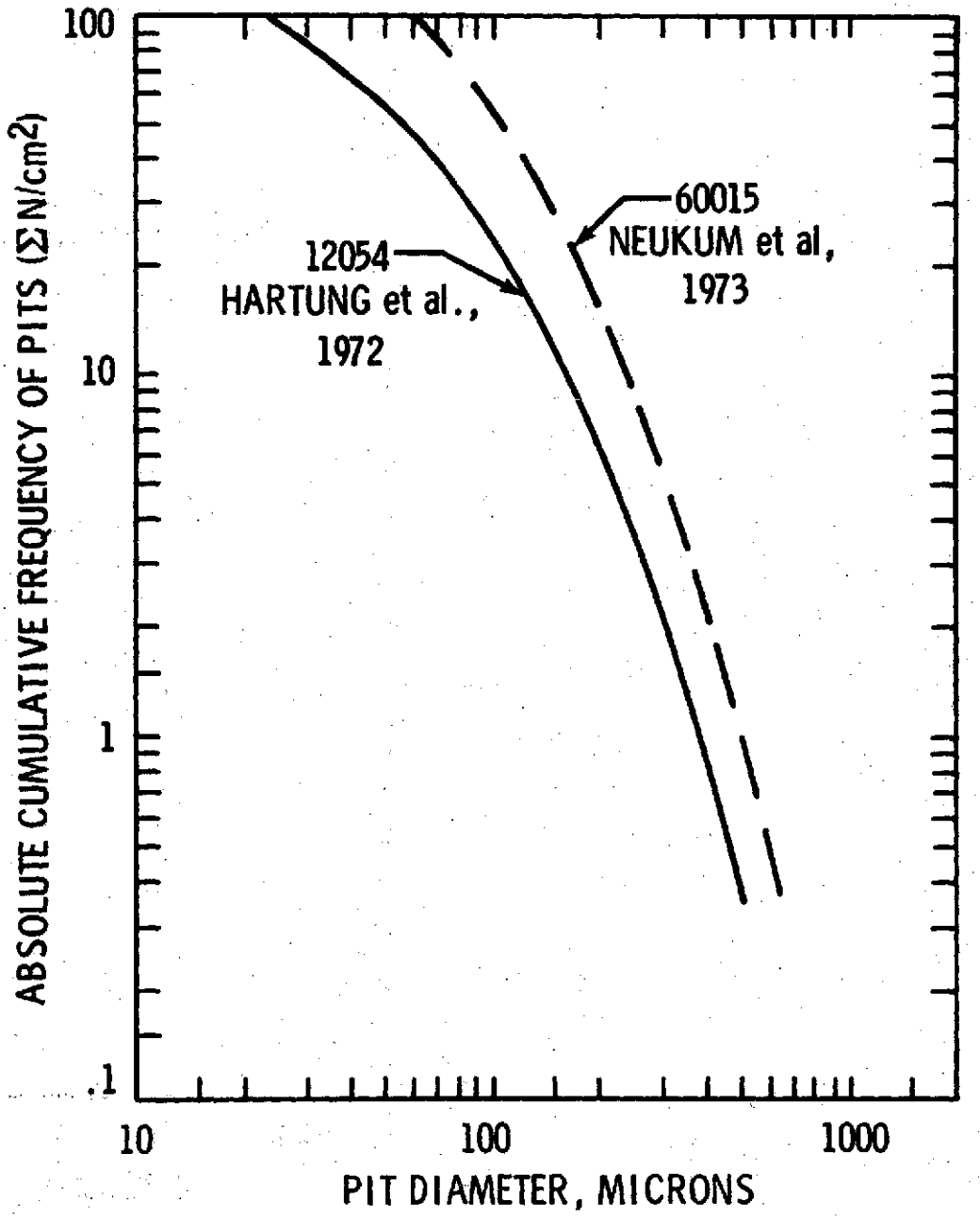
100
10
1
.1
ABSOLUTE CUMULATIVE FREQUENCY OF PITS (ΣN/cm²)
12054
HARTUNG et al.,
1972
60015
NEUKUM et al,
1973
10
100
1000
PIT DIAMETER, MICRONS

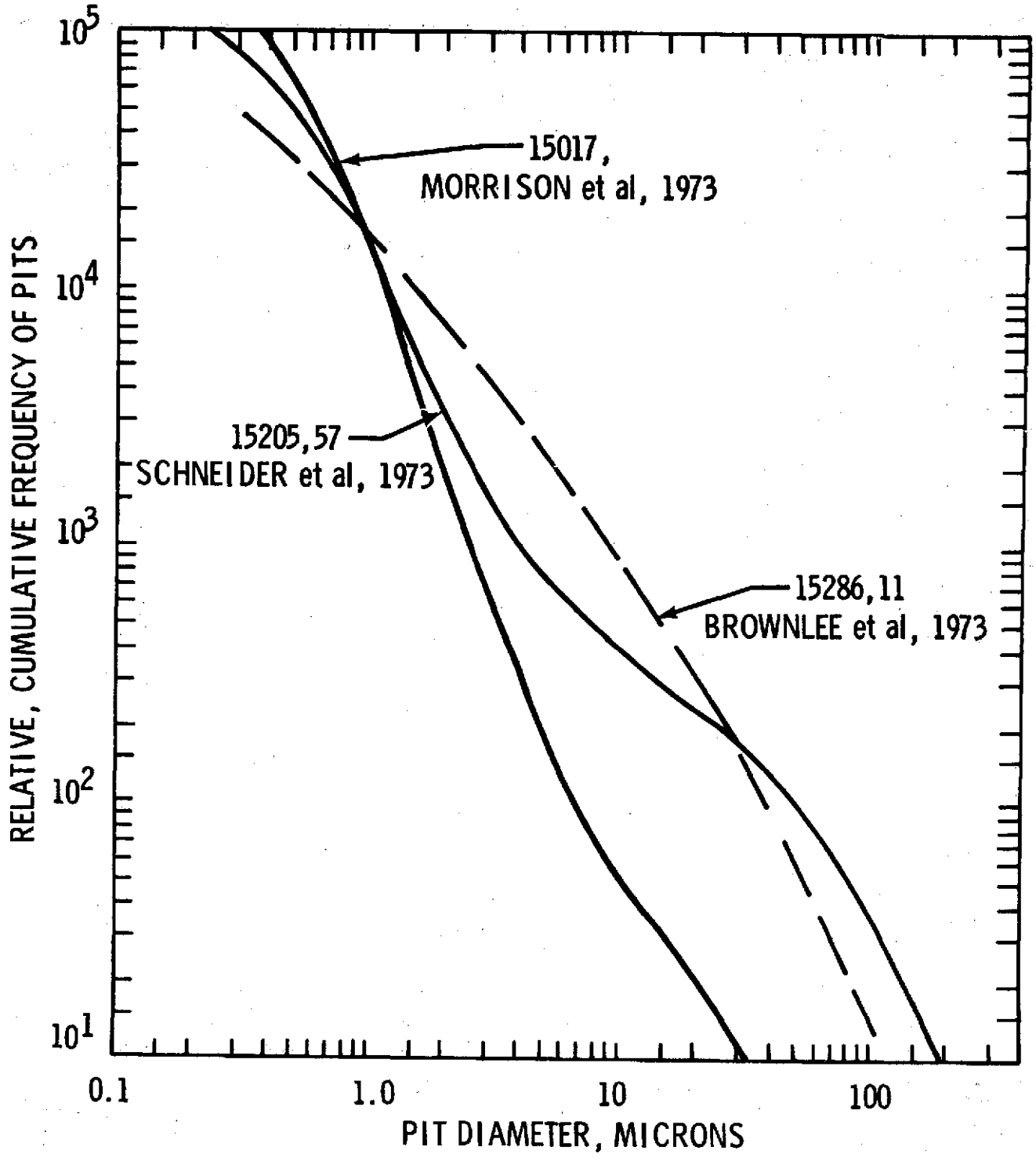
10^5
10^4
10^3
10^2
10^1
RELATIVE, CUMULATIVE FREQUENCY OF PITS
15017,
MORRISON et al, 1973
15205,57
SCHNEIDER et al, 1973
15286,11
BROWNLEE et al, 1973
0.1
1.0
10
100
PIT DIAMETER, MICRONS

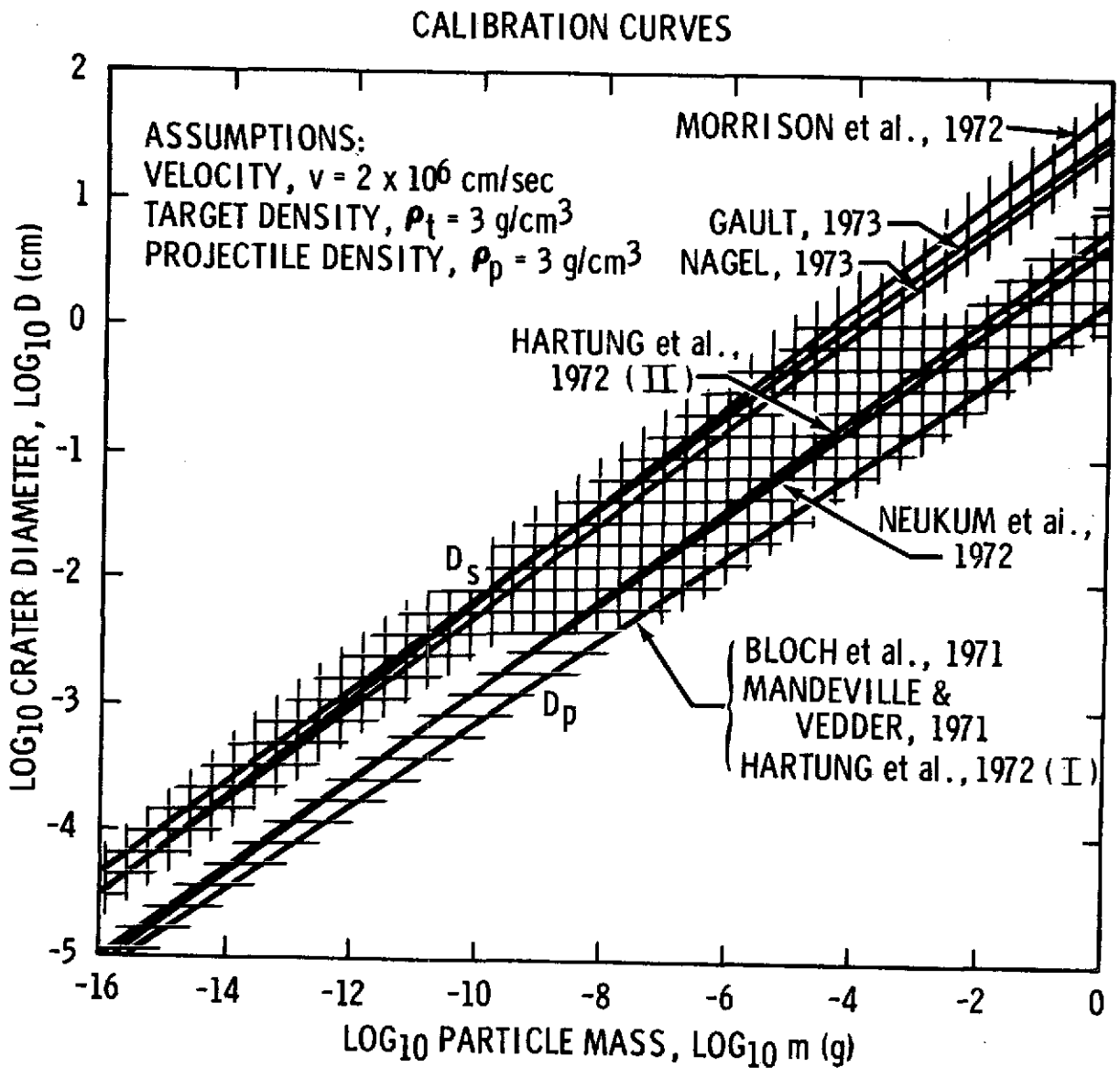
CALIBRATION CURVES
ASSUMPTIONS:
VELOCITY, v = 2 x 10^6 cm/sec
TARGET DENSITY, ρt = 3 g/cm3
PROJECTILE DENSITY, ρp = 3 g/cm3
MORRISON et al., 1972
GAULT, 1973
NAGEL, 1973
HARTUNG et al., 1972 (II)
NEUKUM et al., 1972
Ds
Dp
BLOCH et al., 1971
MANDEVILLE & VEDDER, 1971
HARTUNG et al., 1972 (I)
LOG10 CRATER DIAMETER, LOG10 D (cm)
LOG10 PARTICLE MASS, LOG10 m (g)
2
1
0
-1
-2
-3
-4
-5
-16
-14
-12
-10
-8
-6
-4
-2
0

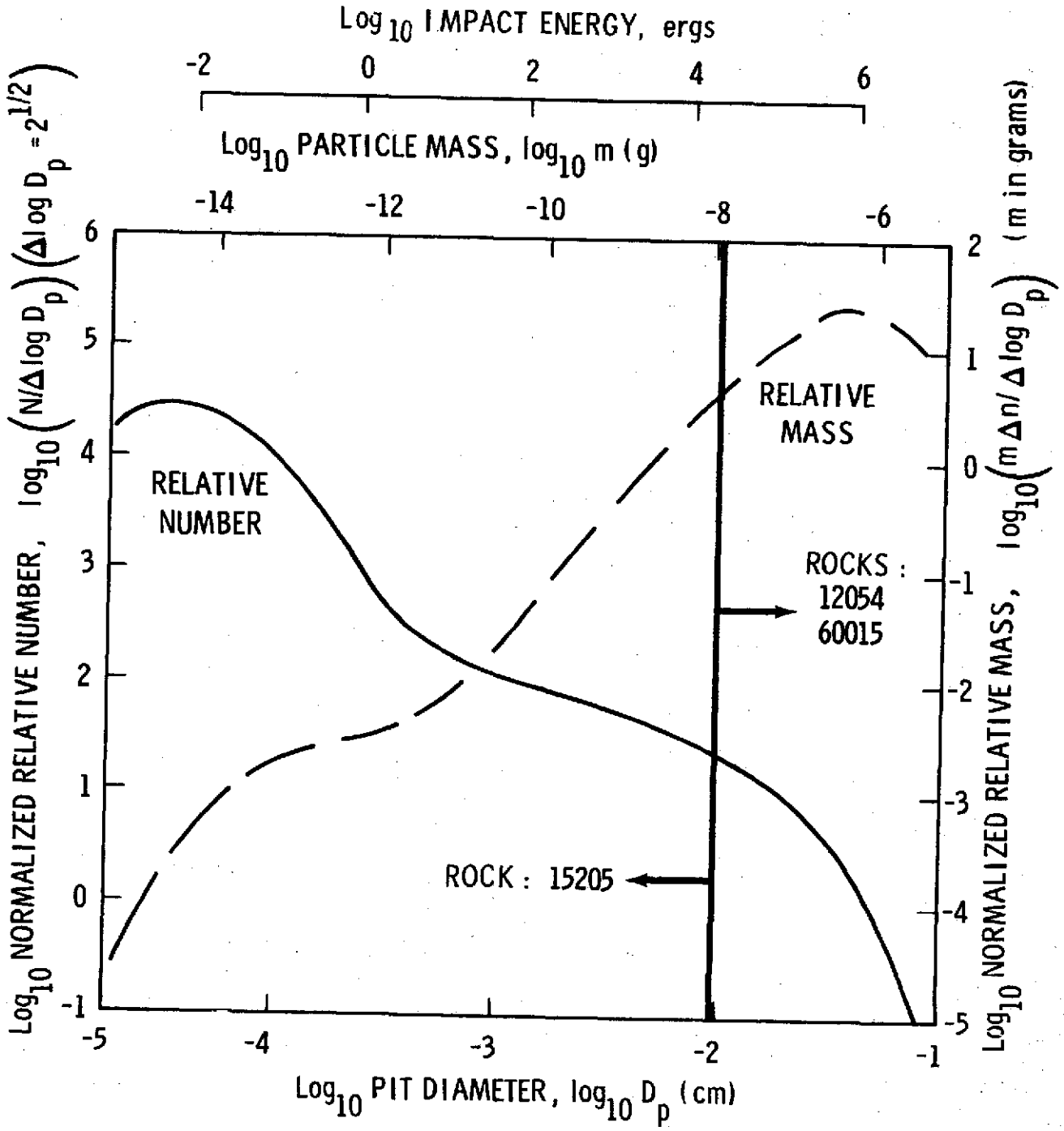
Log 10 IMPACT ENERGY, ergs
-2
0
2
4
6
Log10 PARTICLE MASS, log10 m (g)
-14
-12
-10
-8
-6
Log10 NORMALIZED RELATIVE NUMBER, log10 (N/Δ log Dp) (Δ log Dp = 2^1/2)
6
5
4
3
2
1
0
-1
RELATIVE NUMBER
RELATIVE MASS
ROCKS : 12054 60015
ROCK : 15205
Log10 NORMALIZED RELATIVE MASS, log10 (m Δn/ Δ log Dp) (m in grams)
2
1
0
-1
-2
-3
-4
-5
-5
-4
-3
-2
-1
Log10 PIT DIAMETER, log10 Dp (cm)

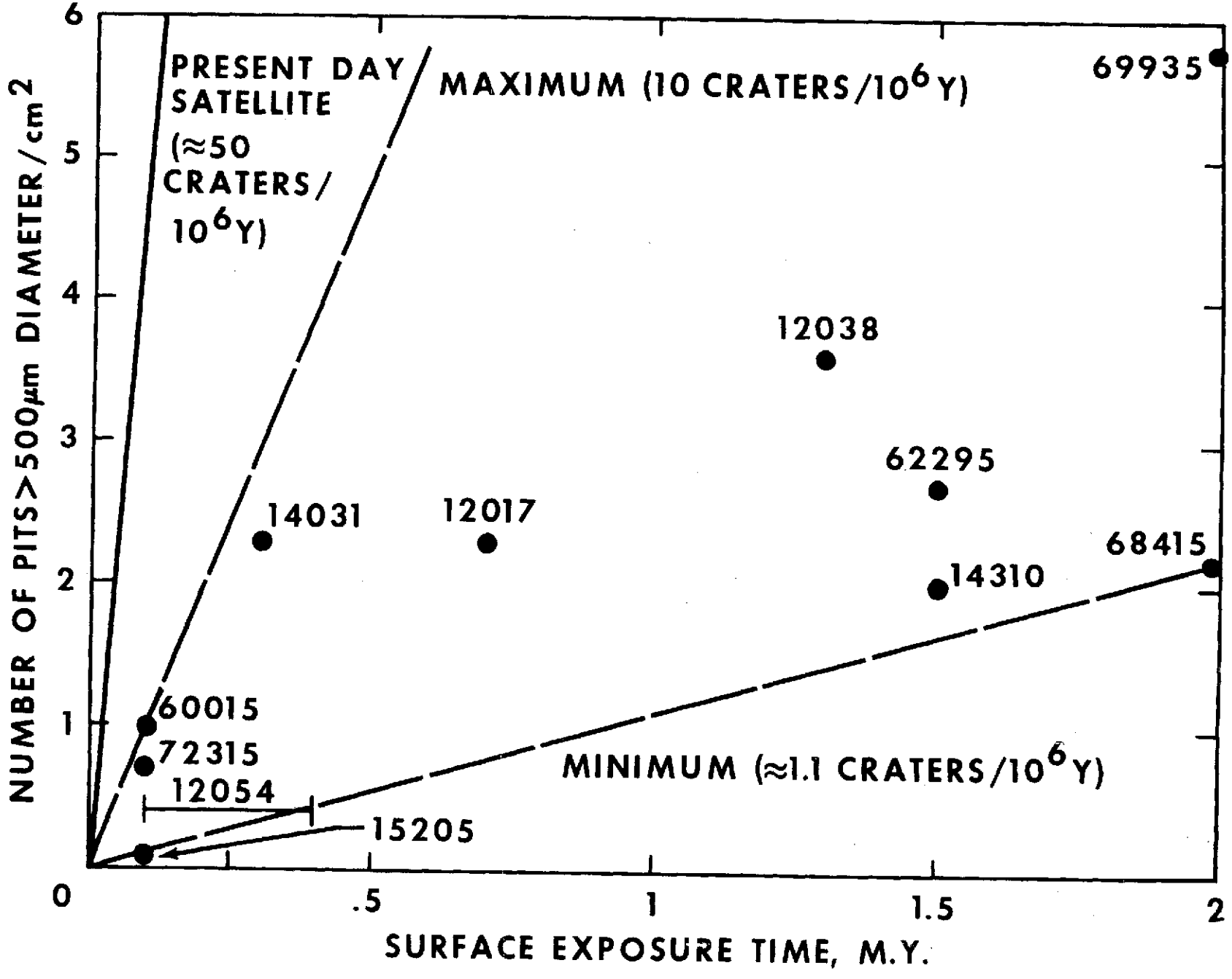
PRESENT DAY SATELLITE (≈50 CRATERS/ 10^6Y)
MAXIMUM (10 CRATERS/10^6Y)
MINIMUM (≈1.1 CRATERS/10^6Y)
69935
12038
62295
14031
12017
68415
14310
60015
72315
12054
15205
NUMBER OF PITS>500μm DIAMETER/cm^2
SURFACE EXPOSURE TIME, M.Y.
0
.5
1
1.5
2
1
2
3
4
5
6

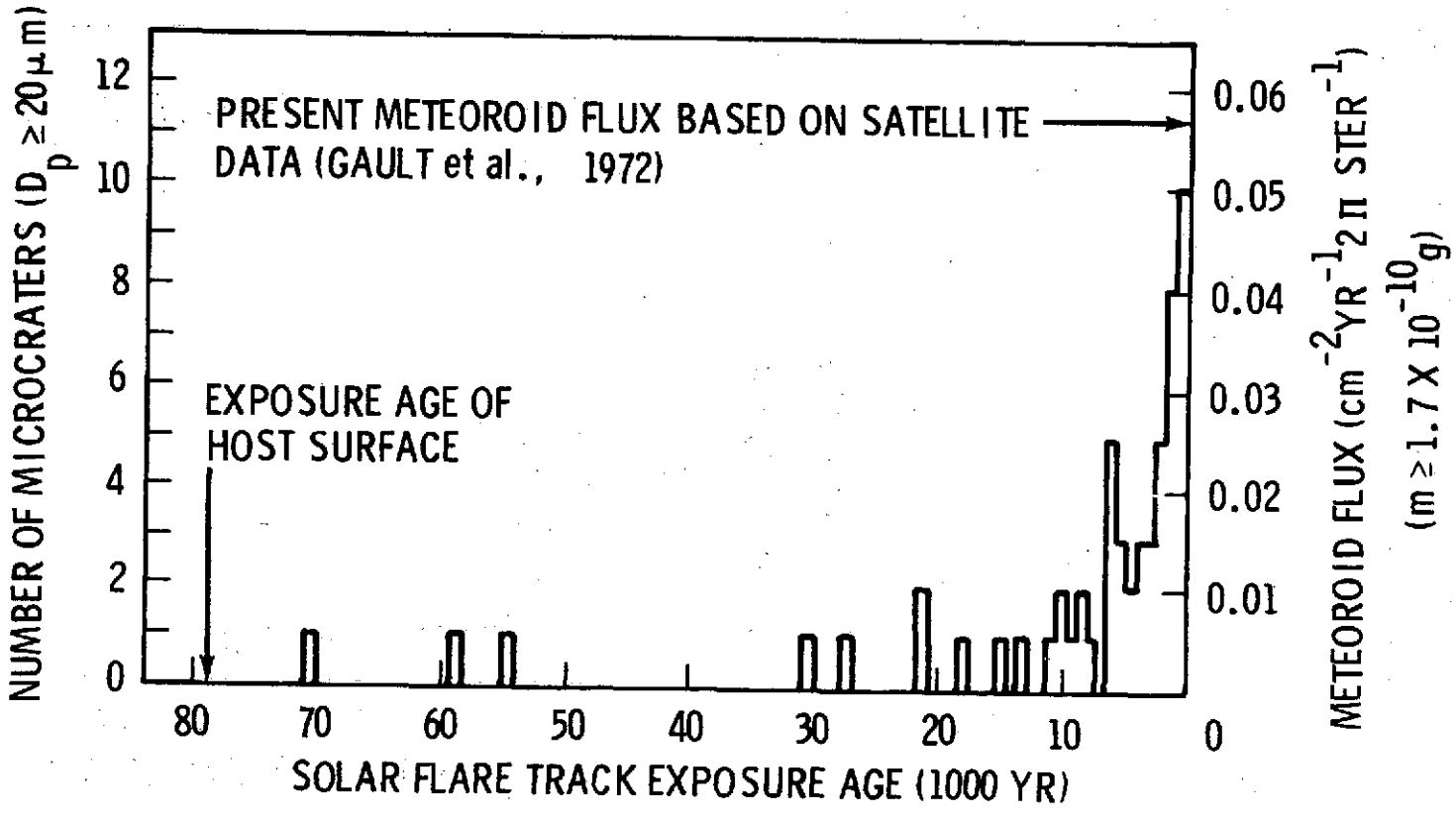
NUMBER OF MICROCRATERS ($D_p \geq 20\mu m$)
12
10
8
6
4
2
0
PRESENT METEOROID FLUX BASED ON SATELLITE DATA (GAULT et al., 1972)
EXPOSURE AGE OF HOST SURFACE
80
70
60
50
40
30
20
10
0
SOLAR FLARE TRACK EXPOSURE AGE (1000 YR)
0.06
0.05
0.04
0.03
0.02
0.01
METEOROID FLUX ($cm^{-2} YR^{-1} 2\pi$ STER^{-1}) ($m \geq 1.7 \times 10^{-10}$ g)

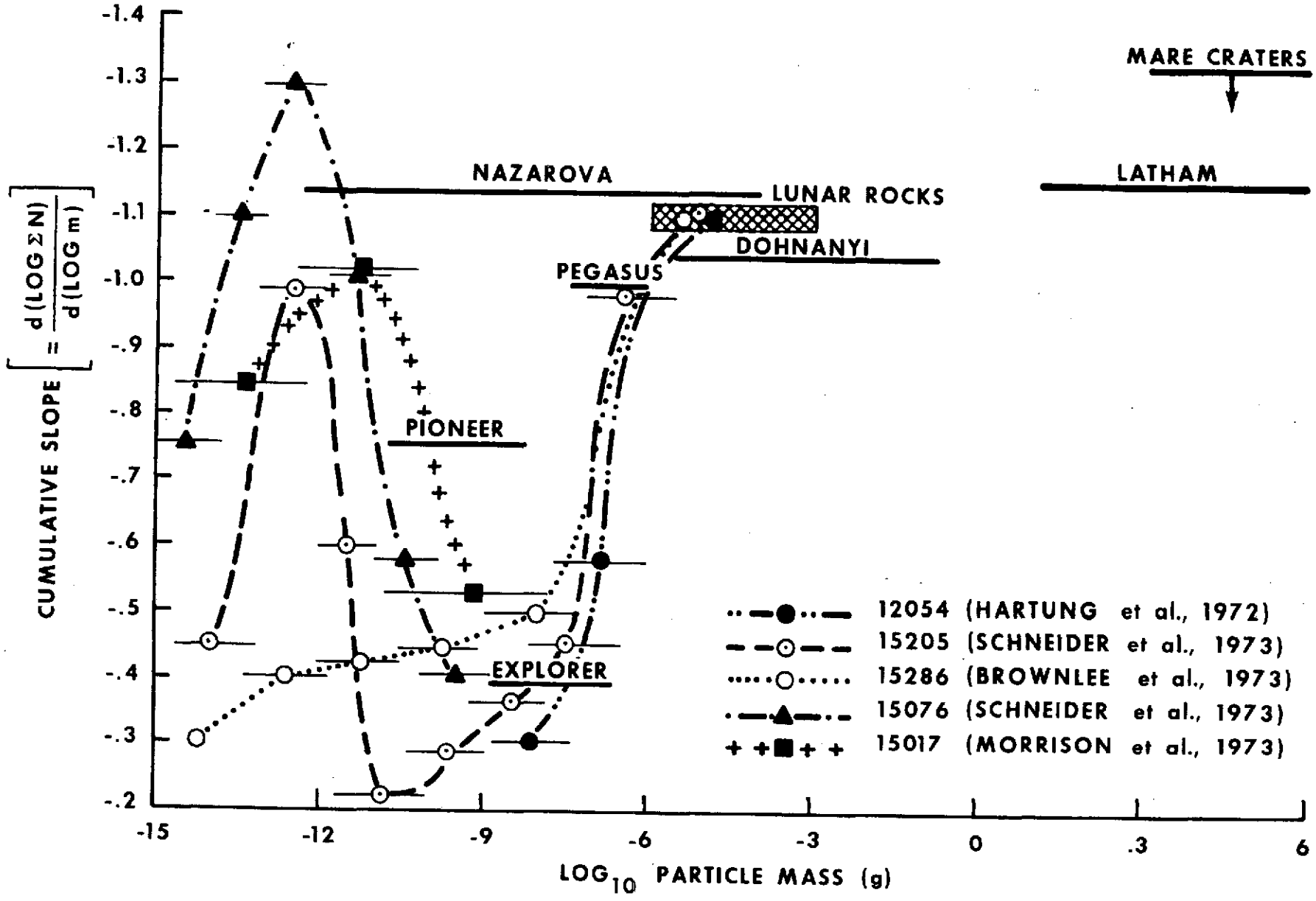
MARE CRATERS
LATHAM
NAZAROVA
LUNAR ROCKS
DOHNANYI
PEGASUS
PIONEER
EXPLORER
12054 (HARTUNG et al., 1972)
15205 (SCHNEIDER et al., 1973)
15286 (BROWNLEE et al., 1973)
15076 (SCHNEIDER et al., 1973)
15017 (MORRISON et al., 1973)
CUMULATIVE SLOPE = d(LOG Σ N) / d(LOG m)
-1.4
-1.3
-1.2
-1.1
-1.0
-.9
-.8
-.7
-.6
-.5
-.4
-.3
-.2
-15
-12
-9
-6
-3
0
.3
6
LOG10 PARTICLE MASS (g)

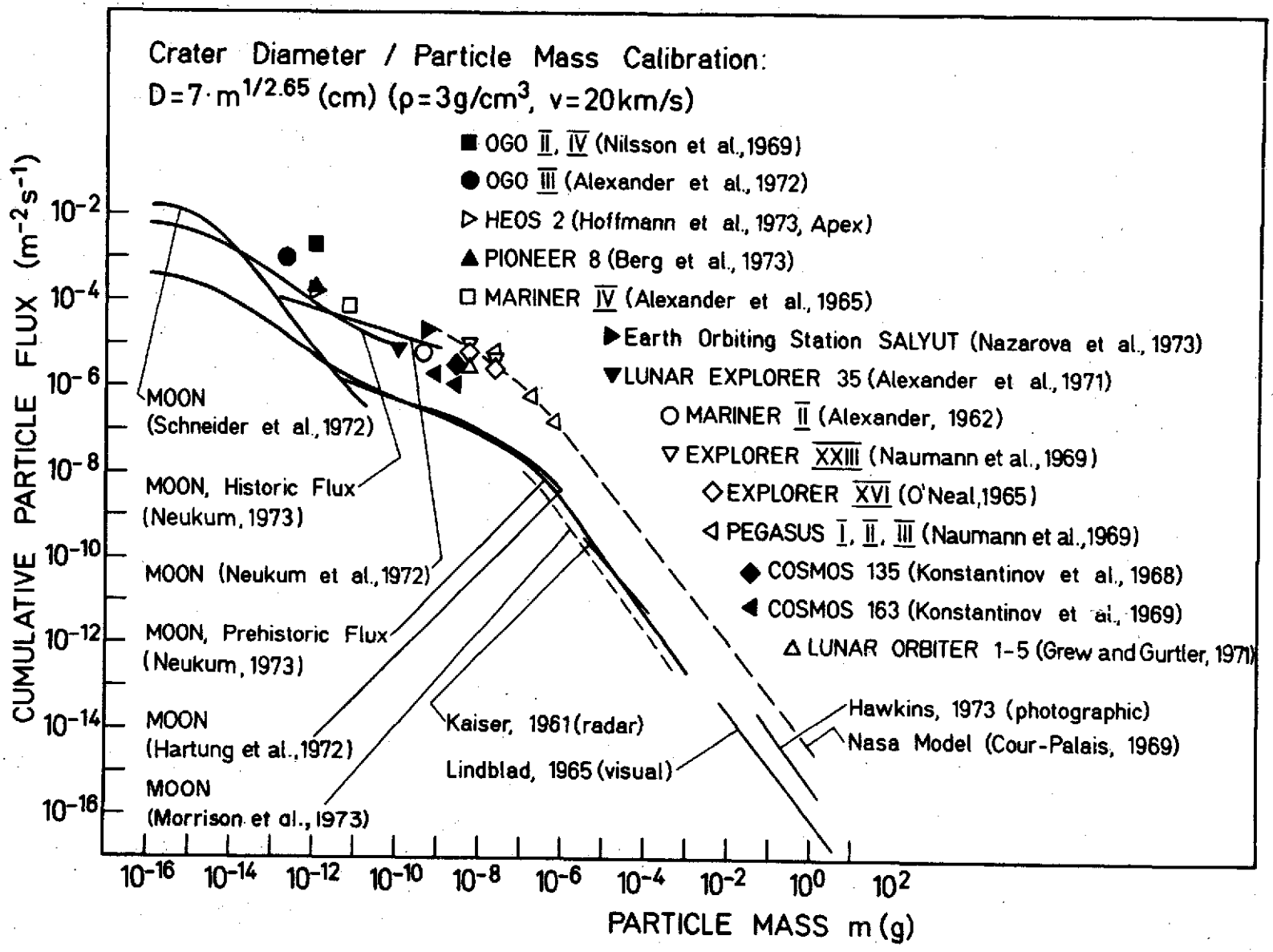
Crater Diameter / Particle Mass Calibration:
D=7·m^1/2.65 (cm) (ρ=3g/cm³, v=20km/s)
OGO II, IV (Nilsson et al.,1969)
OGO III (Alexander et al., 1972)
HEOS 2 (Hoffmann et al., 1973, Apex)
PIONEER 8 (Berg et al., 1973)
MARINER IV (Alexander et al., 1965)
Earth Orbiting Station SALYUT (Nazarova et al., 1973)
LUNAR EXPLORER 35 (Alexander et al., 1971)
MARINER II (Alexander, 1962)
EXPLORER XXIII (Naumann et al., 1969)
EXPLORER XVI (O'Neal,1965)
PEGASUS I, II, III (Naumann et al.,1969)
COSMOS 135 (Konstantinov et al., 1968)
COSMOS 163 (Konstantinov et al., 1969)
LUNAR ORBITER 1-5 (Grew and Gurtler, 1971)
MOON (Schneider et al., 1972)
MOON, Historic Flux (Neukum, 1973)
MOON (Neukum et al., 1972)
MOON, Prehistoric Flux (Neukum, 1973)
MOON (Hartung et al., 1972)
MOON (Morrison et al., 1973)
Kaiser, 1961 (radar)
Lindblad, 1965 (visual)
Hawkins, 1973 (photographic)
Nasa Model (Cour-Palais, 1969)
CUMULATIVE PARTICLE FLUX (m⁻²s⁻¹)
10⁻² 10⁻⁴ 10⁻⁶ 10⁻⁸ 10⁻¹⁰ 10⁻¹² 10⁻¹⁴ 10⁻¹⁶
10⁻¹⁶ 10⁻¹⁴ 10⁻¹² 10⁻¹⁰ 10⁻⁸ 10⁻⁶ 10⁻⁴ 10⁻² 10⁰ 10²
PARTICLE MASS m (g)

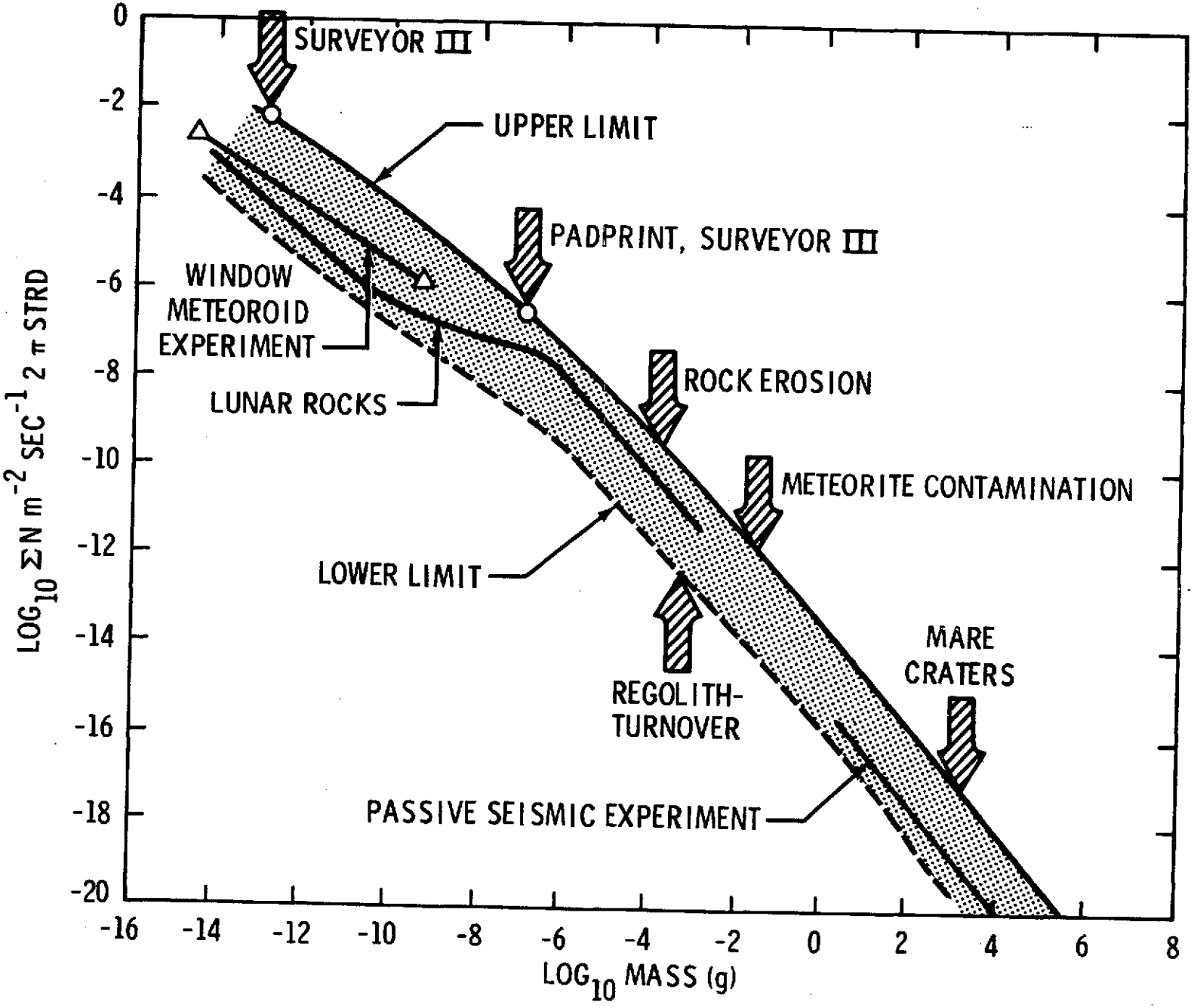
SURVEYOR III
UPPER LIMIT
PADPRINT, SURVEYOR III
WINDOW METEOROID EXPERIMENT
LUNAR ROCKS
ROCK EROSION
METEORITE CONTAMINATION
LOWER LIMIT
REGOLITH-TURNOVER
MARE CRATERS
PASSIVE SEISMIC EXPERIMENT
$LOG_{10} \Sigma N\ m^{-2}\ SEC^{-1}\ 2\pi\ STRD$
LOG_{10} MASS (g)
0
-2
-4
-6
-8
-10
-12
-14
-16
-18
-20
-16
-14
-12
-10
-8
-6
-4
-2
0
2
4
6
8

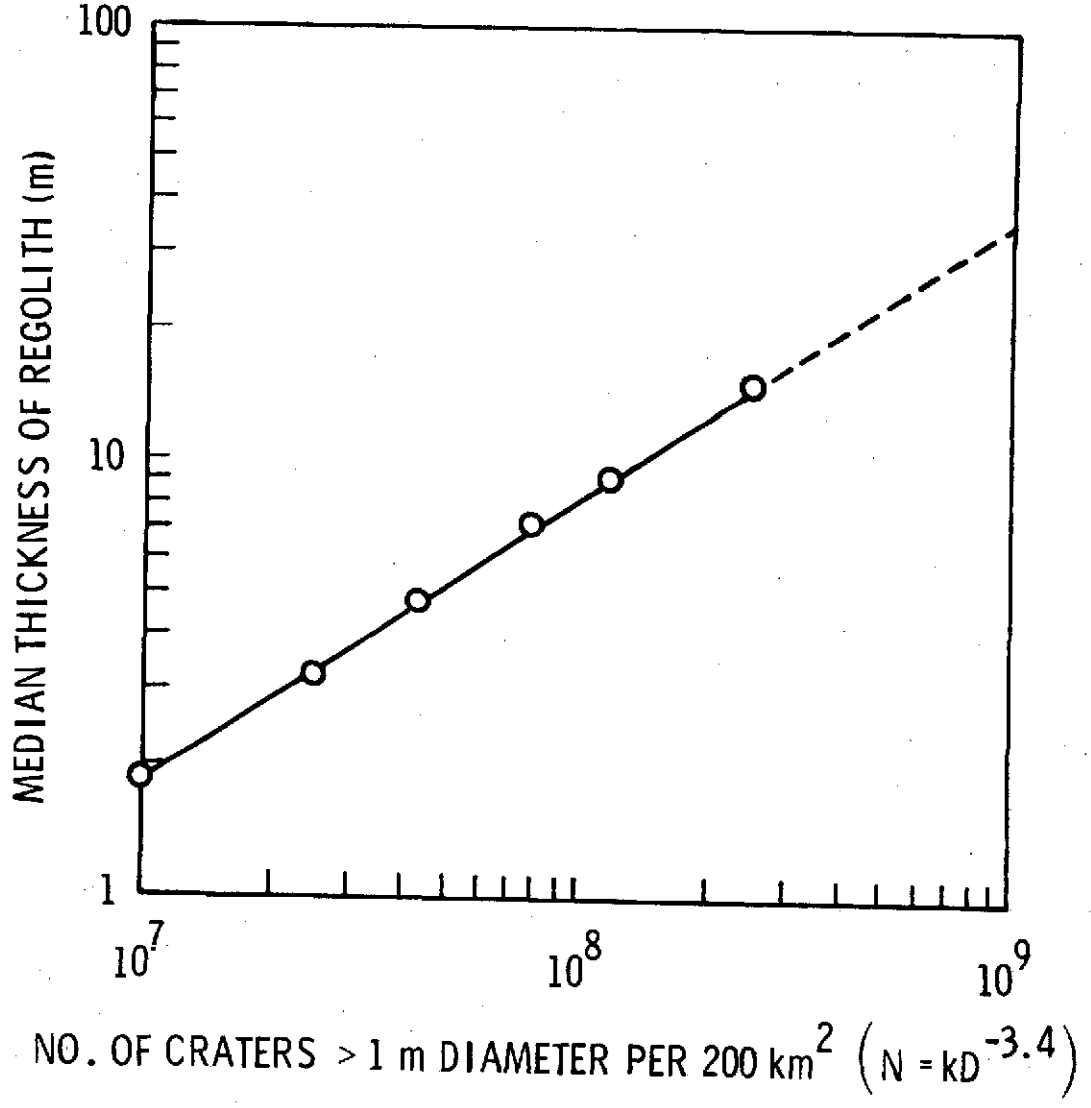
100
10
1
MEDIAN THICKNESS OF REGOLITH (m)
10^7
10^8
10^9
NO. OF CRATERS > 1 m DIAMETER PER 200 km^2 ($N = kD^{-3.4}$)

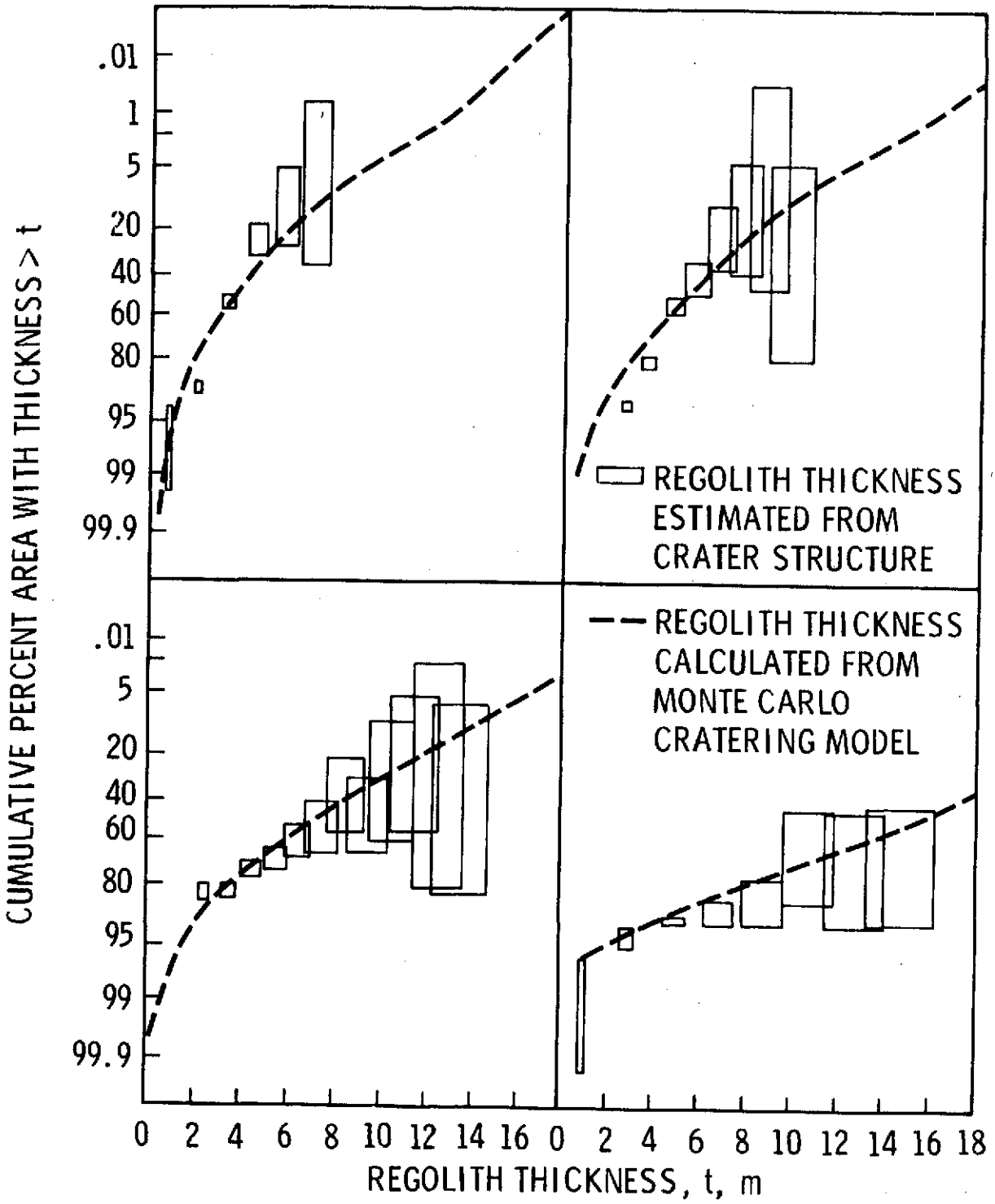
CUMULATIVE PERCENT AREA WITH THICKNESS > t
.01
1
5
20
40
60
80
95
99
99.9
.01
5
20
40
60
80
95
99
99.9
REGOLITH THICKNESS ESTIMATED FROM CRATER STRUCTURE
REGOLITH THICKNESS CALCULATED FROM MONTE CARLO CRATERING MODEL
0 2 4 6 8 10 12 14 16
0 2 4 6 8 10 12 14 16 18
REGOLITH THICKNESS, t, m

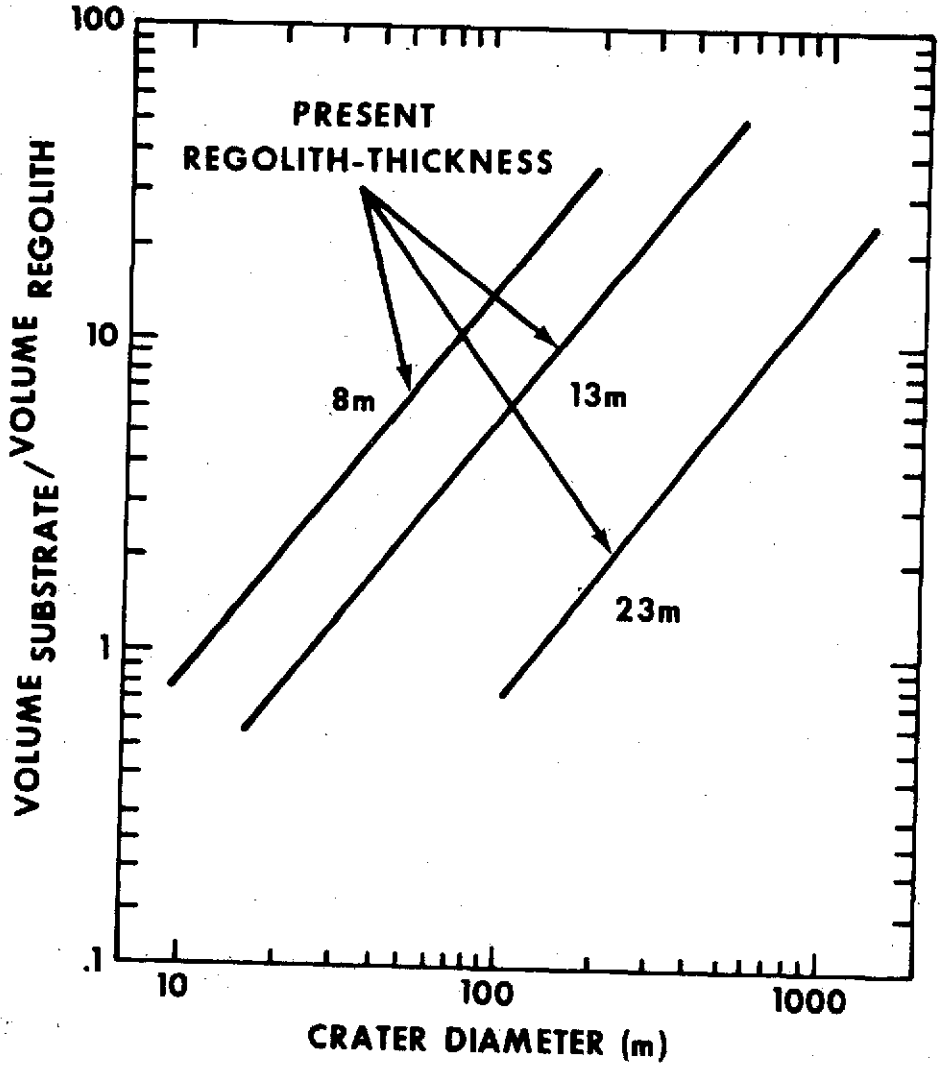
100
10
1
.1
PRESENT
REGOLITH-THICKNESS
8m
13m
23m
VOLUME SUBSTRATE/VOLUME REGOLITH
10
100
1000
CRATER DIAMETER (m)

PERCENT OF TOTAL REGOLITH DEBRIS
DERIVED FROM ORIGINAL DEPTH > d
0
20
40
60
80
100
1
10
100
1000
DEPTH, d, m

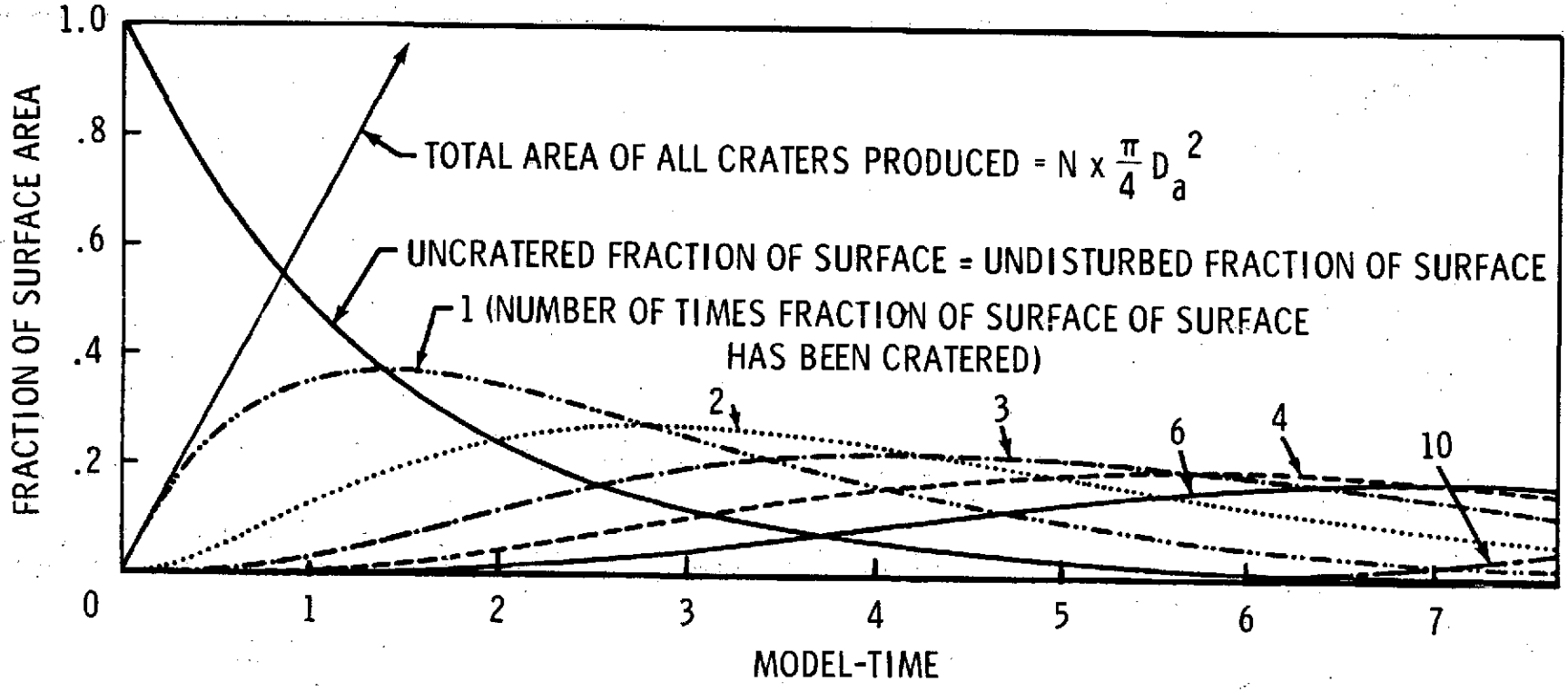
1.0
.8
.6
.4
.2
0
FRACTION OF SURFACE AREA
TOTAL AREA OF ALL CRATERS PRODUCED = N x π/4 D_a^2
UNCRATERED FRACTION OF SURFACE = UNDISTURBED FRACTION OF SURFACE
1 (NUMBER OF TIMES FRACTION OF SURFACE OF SURFACE HAS BEEN CRATERED)
2
3
6
4
10
1
2
3
4
5
6
7
MODEL-TIME

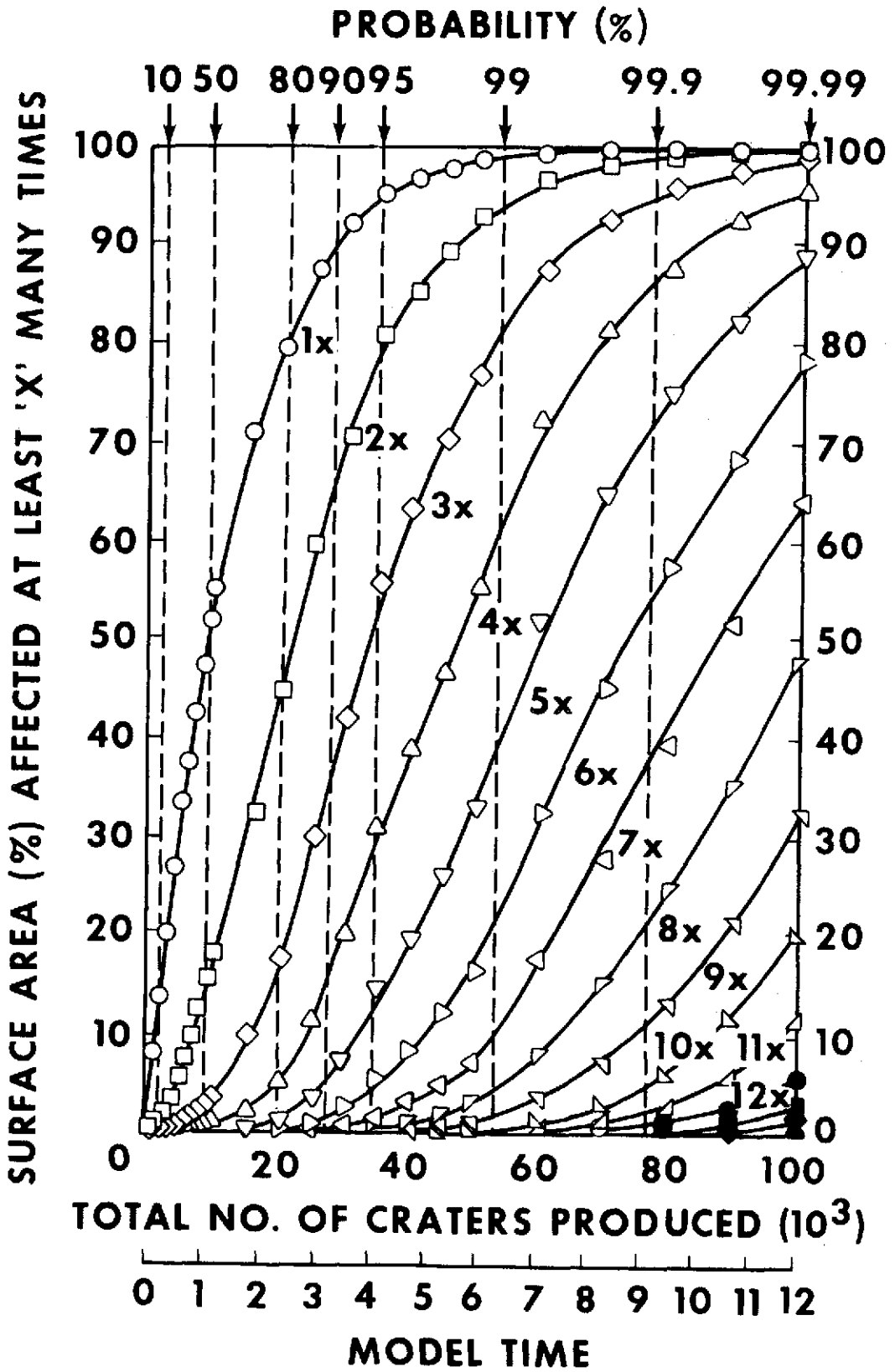
PROBABILITY (%)
10 50 80 90 95 99 99.9 99.99
SURFACE AREA (%) AFFECTED AT LEAST 'X' MANY TIMES
100
90
80
70
60
50
40
30
20
10
0
1x
2x
3x
4x
5x
6x
7x
8x
9x
10x
11x
12x
0 20 40 60 80 100
TOTAL NO. OF CRATERS PRODUCED (10^3)
0 1 2 3 4 5 6 7 8 9 10 11 12
MODEL TIME

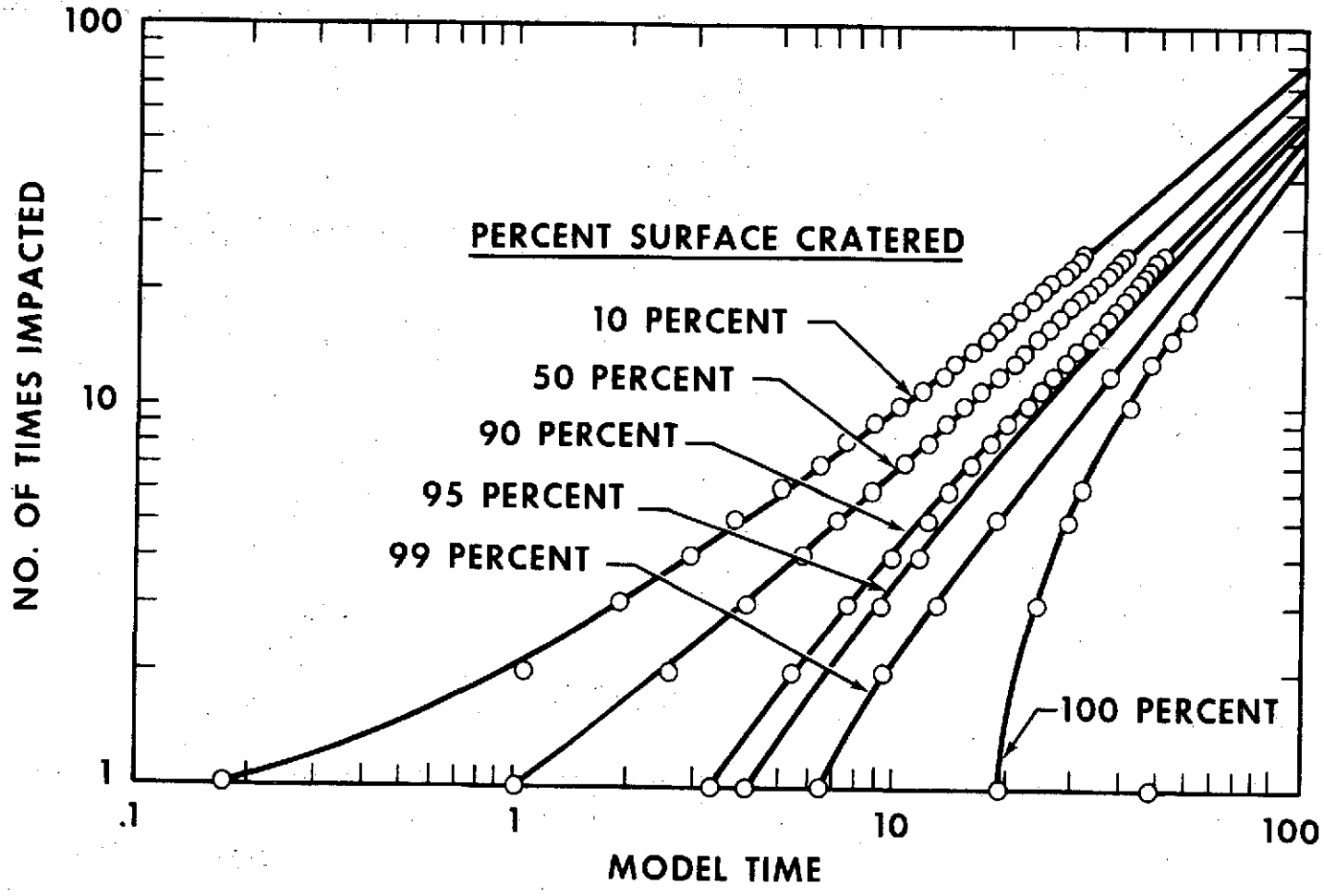
100
10
1
.1
1
10
100
NO. OF TIMES IMPACTED
MODEL TIME
PERCENT SURFACE CRATERED
10 PERCENT
50 PERCENT
90 PERCENT
95 PERCENT
99 PERCENT
100 PERCENT

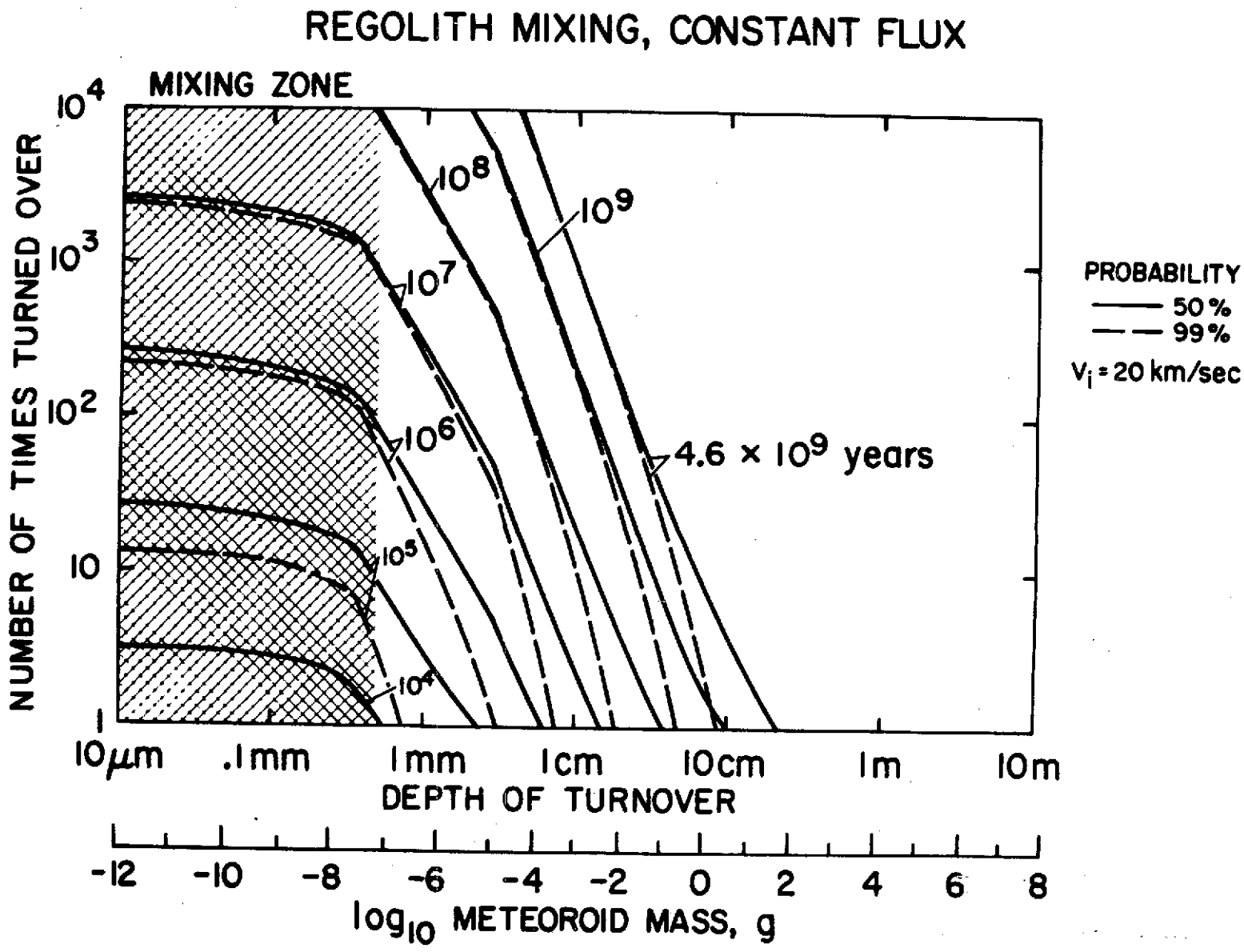
REGOLITH MIXING, CONSTANT FLUX
MIXING ZONE
NUMBER OF TIMES TURNED OVER
10^4
10^3
10^2
10
1
10^8
10^9
10^7
10^6
10^5
10^4
4.6 × 10^9 years
PROBABILITY
50%
99%
V_i = 20 km/sec
10μm
.1mm
1mm
1cm
10cm
1m
10m
DEPTH OF TURNOVER
-12
-10
-8
-6
-4
-2
0
2
4
6
8
log10 METEOROID MASS, g

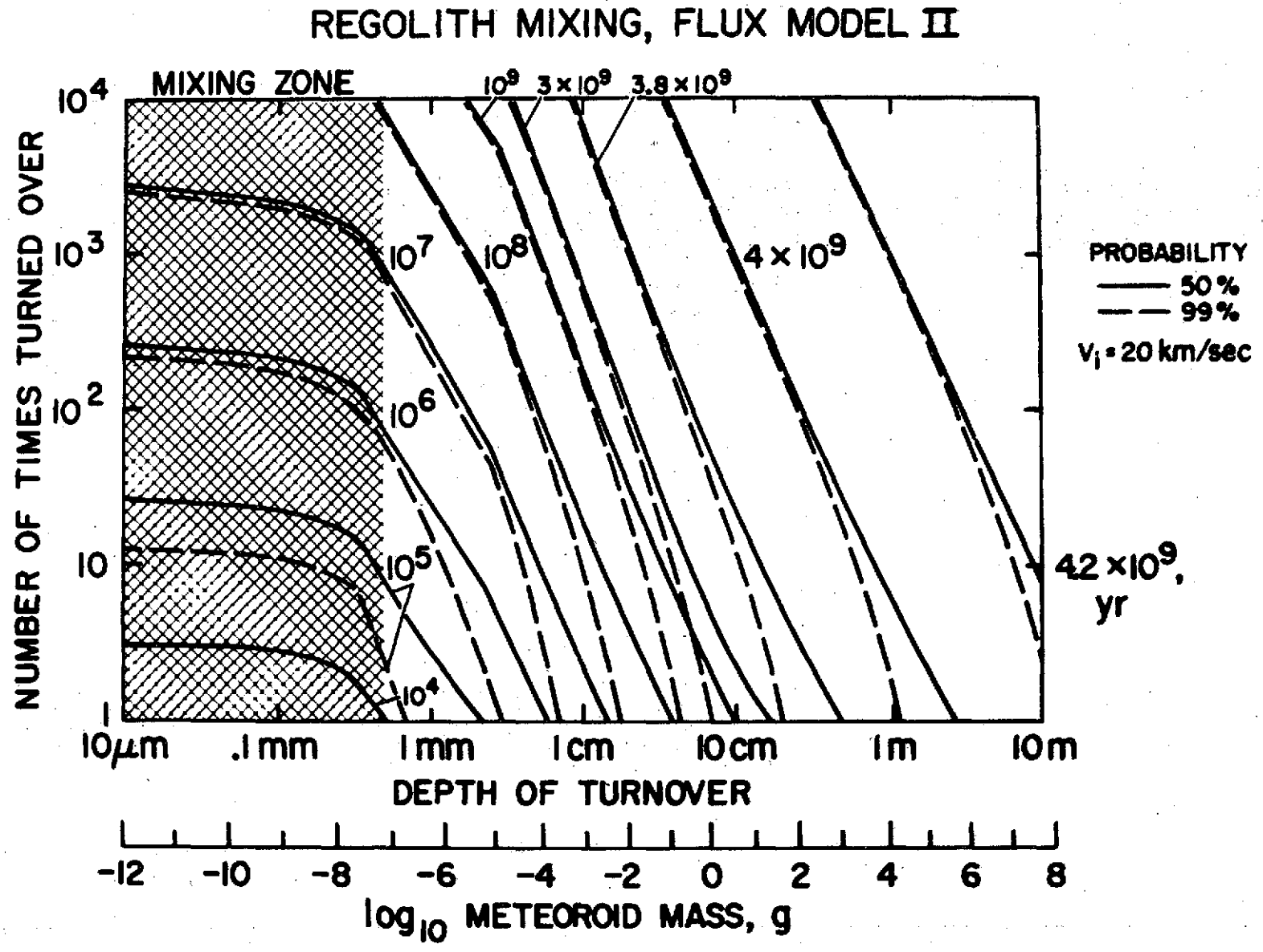
REGOLITH MIXING, FLUX MODEL II
MIXING ZONE
10⁹
3×10⁹
3.8×10⁹
10⁷
10⁸
4×10⁹
10⁶
10⁵
10⁴
4.2×10⁹, yr
PROBABILITY
50%
99%
V∞ = 20 km/sec
NUMBER OF TIMES TURNED OVER
10⁴
10³
10²
10
1
10μm
.1mm
1mm
1cm
10cm
1m
10m
DEPTH OF TURNOVER
-12
-10
-8
-6
-4
-2
0
2
4
6
8
log₁₀ METEOROID MASS, g

NASA
S-72-20932

ROCK 14310

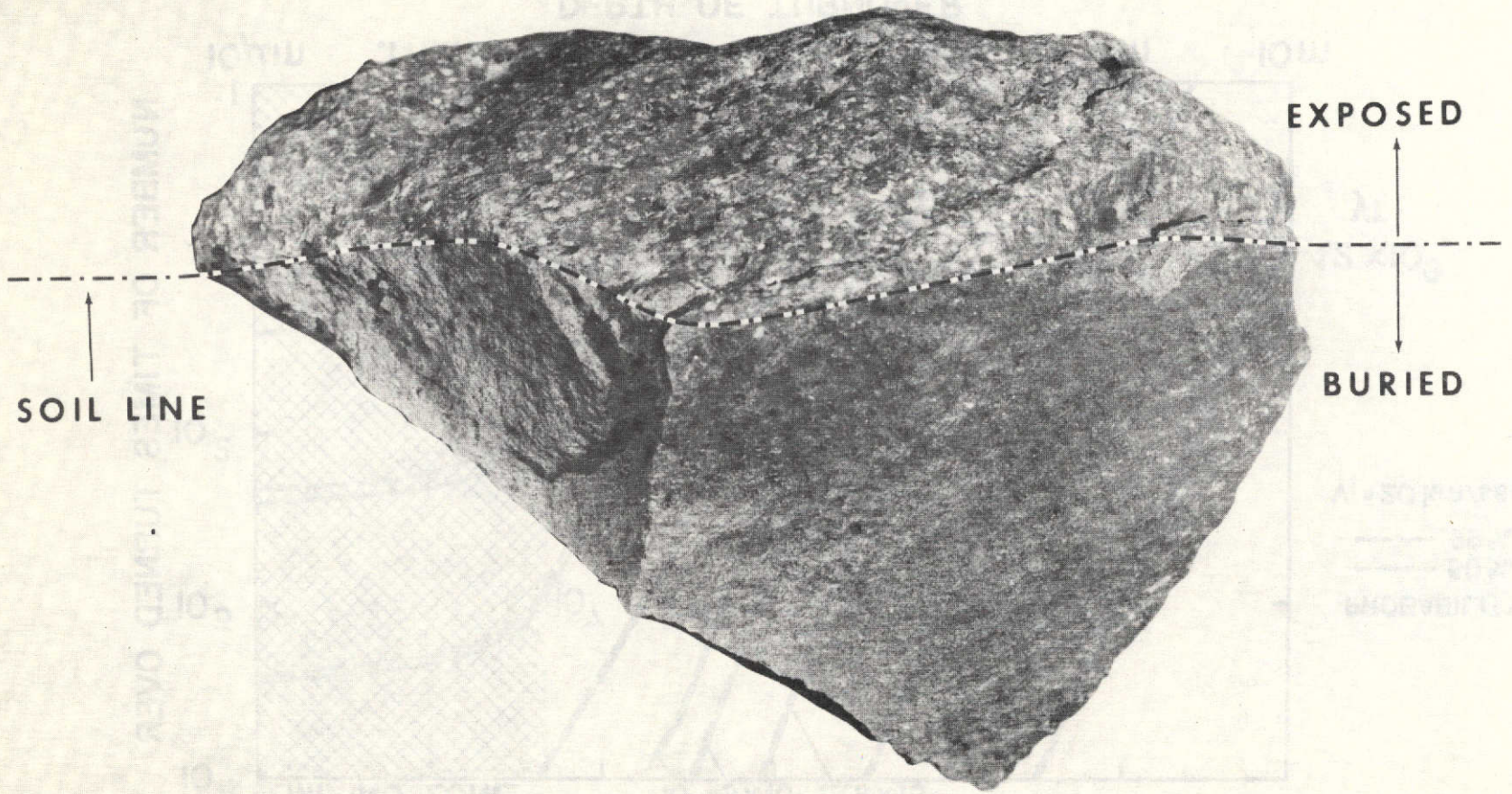

Fig. 24

NASA
S- 73- 23896

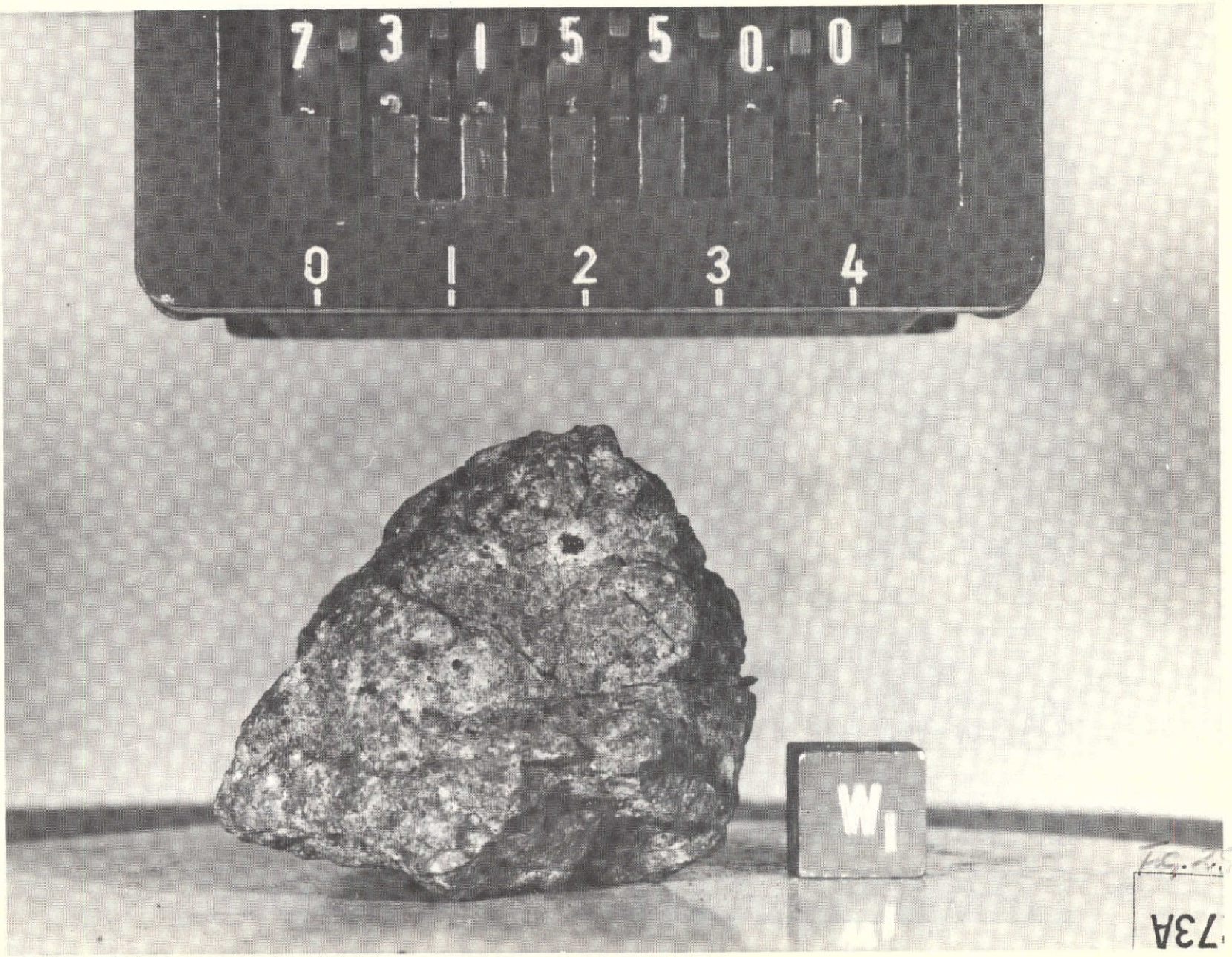

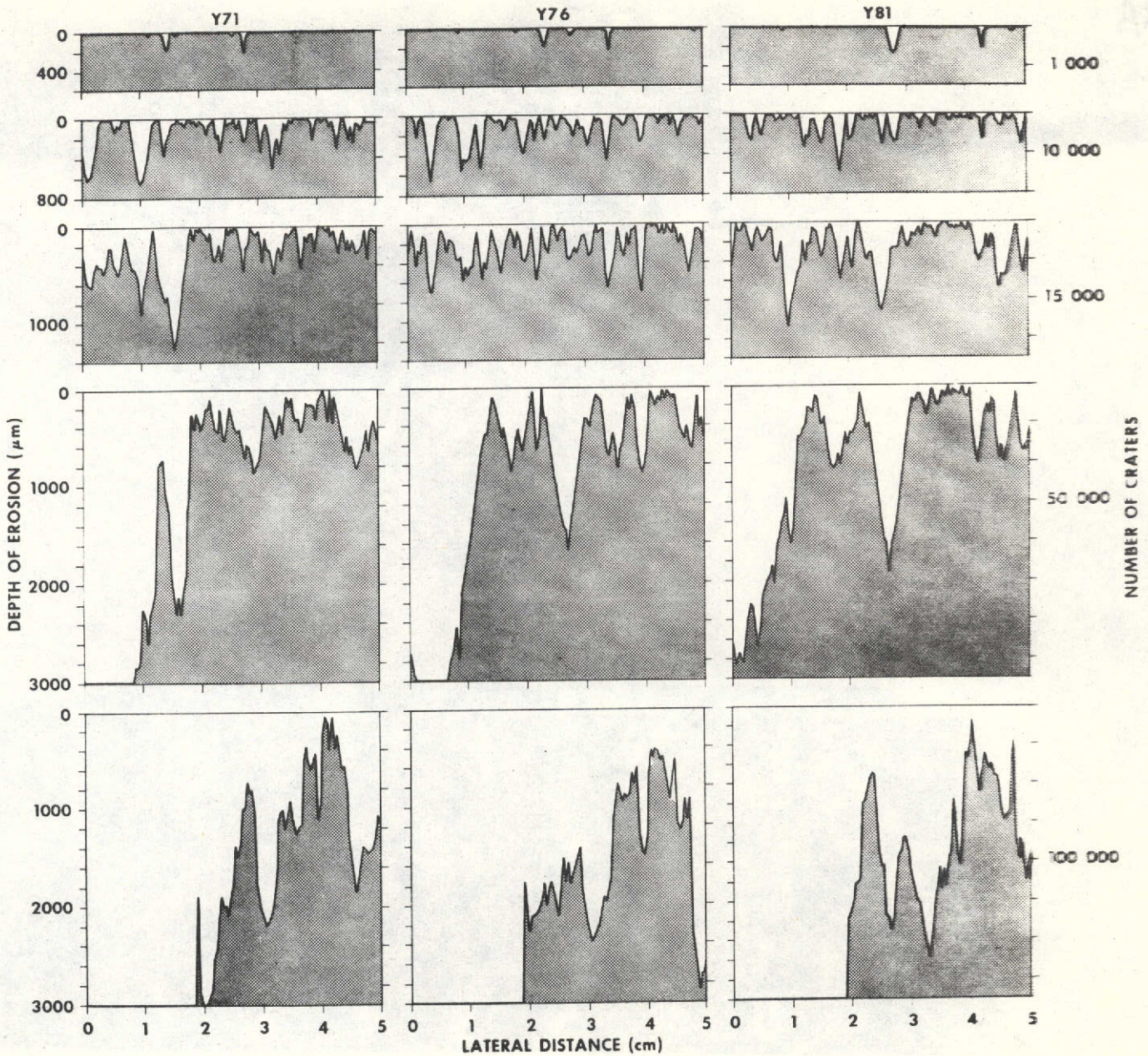
Y71
Y76
Y81
0
400
800
1000
2000
3000
1 000
10 000
15 000
50 000
100 000
DEPTH OF EROSION (μm)
NUMBER OF CRATERS
0
1
2
3
4
5
LATERAL DISTANCE (cm)

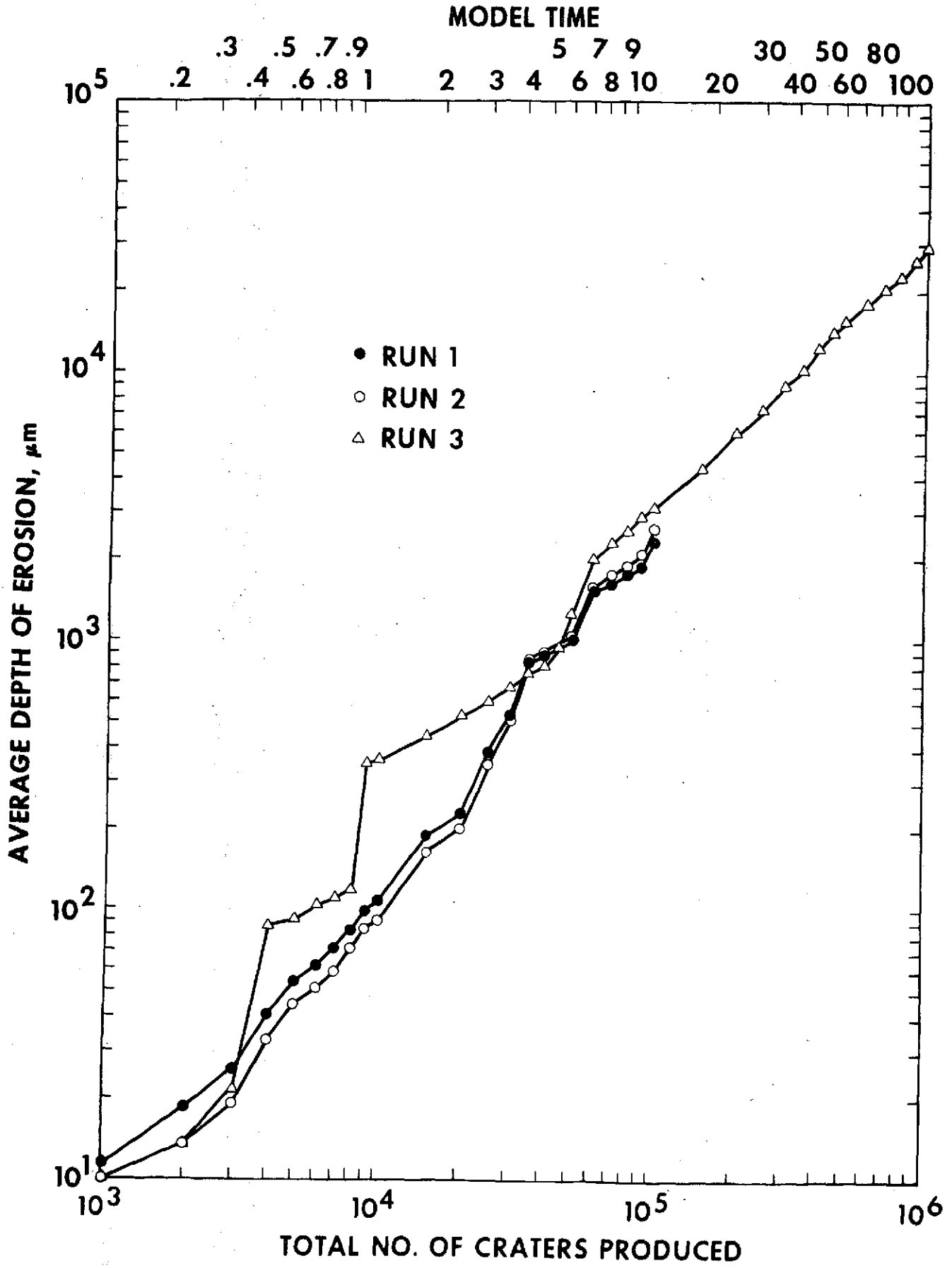
MODEL TIME
.3 .5 .7 .9 5 7 9 30 50 80
.2 .4 .6 .8 1 2 3 4 6 8 10 20 40 60 100
10^5
10^4
10^3
10^2
10^1
RUN 1
RUN 2
RUN 3
AVERAGE DEPTH OF EROSION, μm
10^3
10^4
10^5
10^6
TOTAL NO. OF CRATERS PRODUCED

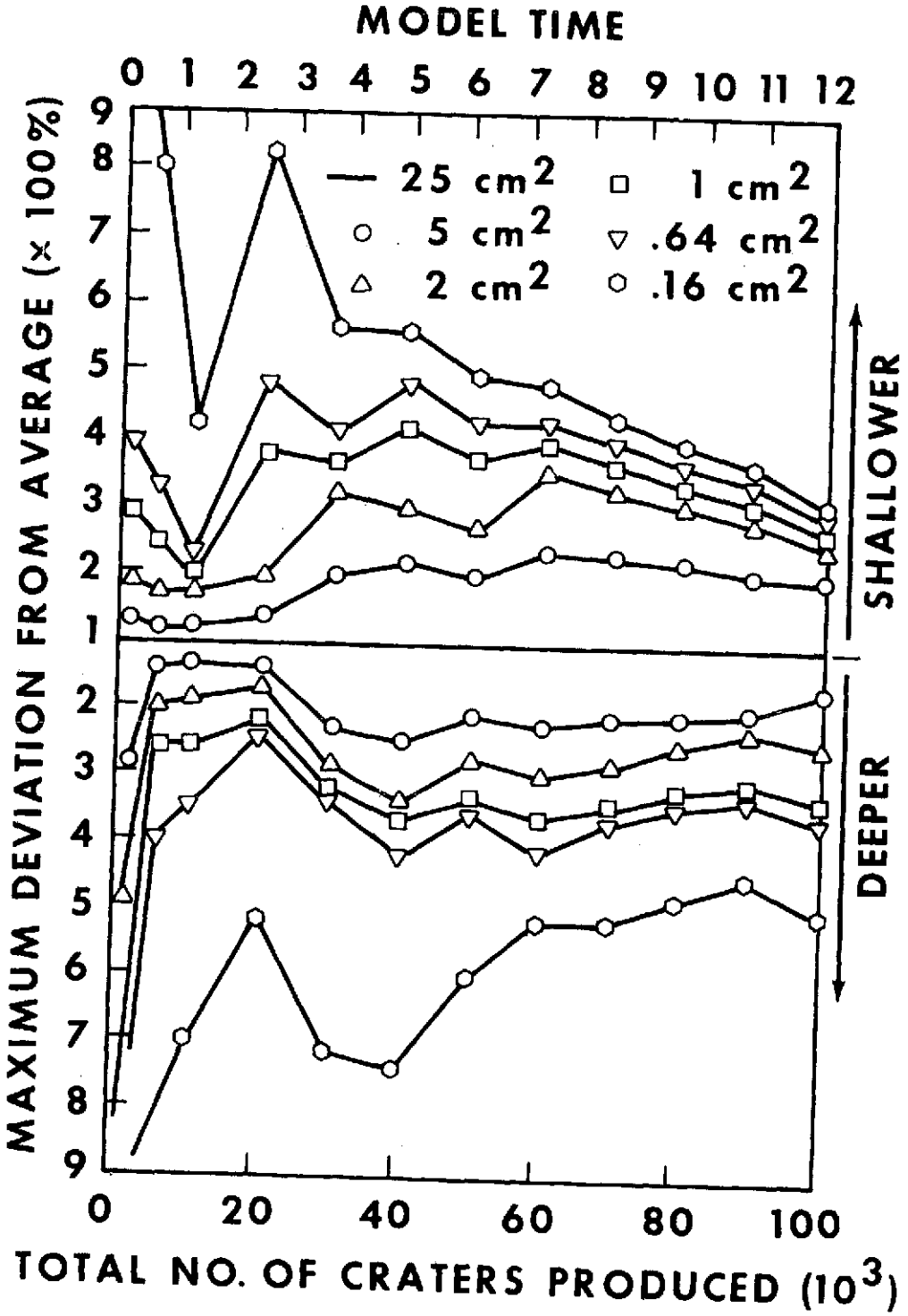
MODEL TIME
0 1 2 3 4 5 6 7 8 9 10 11 12
25 cm2
1 cm2
5 cm2
.64 cm2
2 cm2
.16 cm2
SHALLOWER
DEEPER
MAXIMUM DEVIATION FROM AVERAGE (× 100%)
9 8 7 6 5 4 3 2 1 2 3 4 5 6 7 8 9
0 20 40 60 80 100
TOTAL NO. OF CRATERS PRODUCED (10^3)

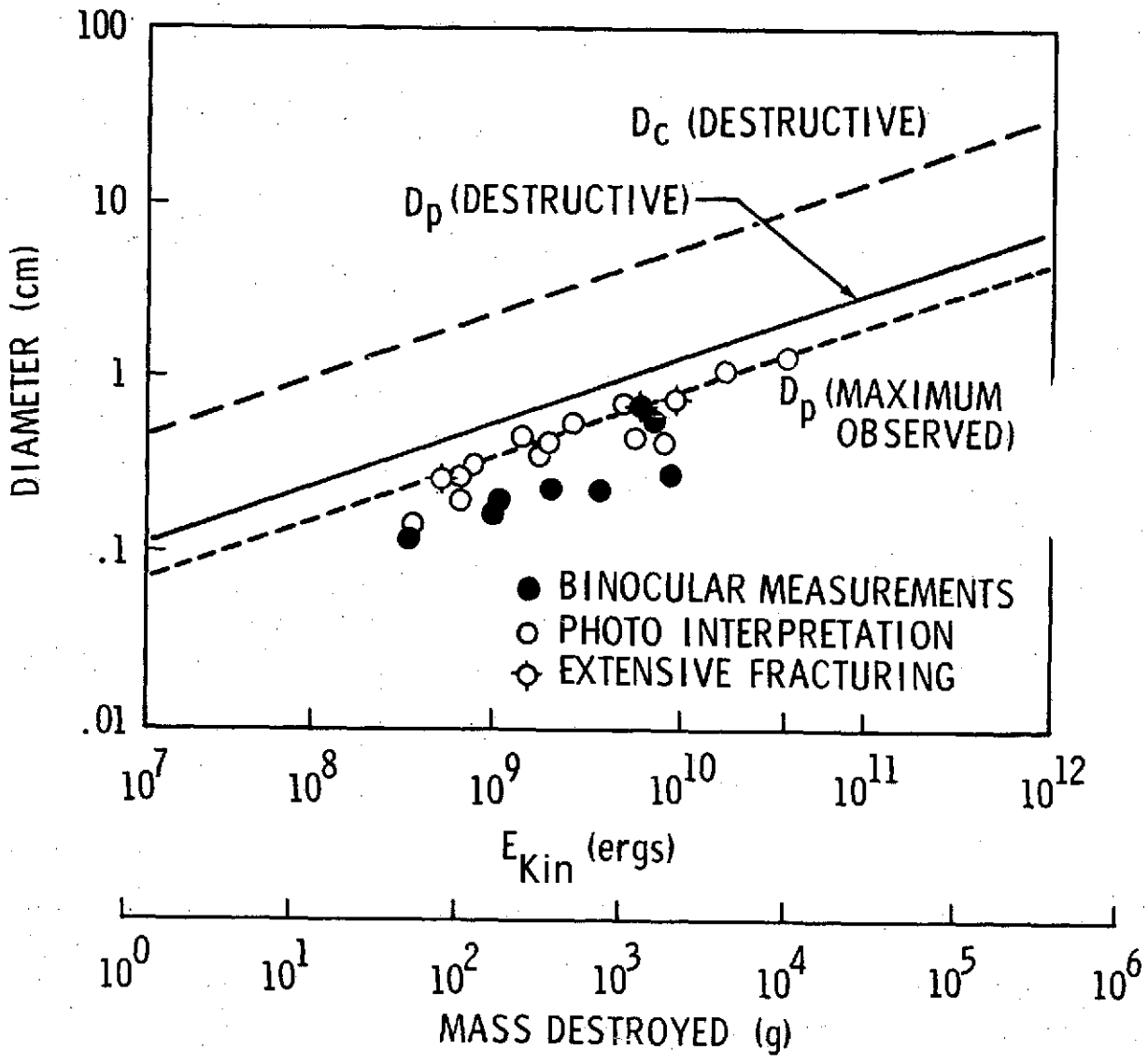
100
10
1
.1
.01
DIAMETER (cm)
D_c (DESTRUCTIVE)
D_p (DESTRUCTIVE)
D_p (MAXIMUM OBSERVED)
BINOCULAR MEASUREMENTS
PHOTO INTERPRETATION
EXTENSIVE FRACTURING
10^7 10^8 10^9 10^{10} 10^{11} 10^{12}
E_{Kin} (ergs)
10^0 10^1 10^2 10^3 10^4 10^5 10^6
MASS DESTROYED (g)

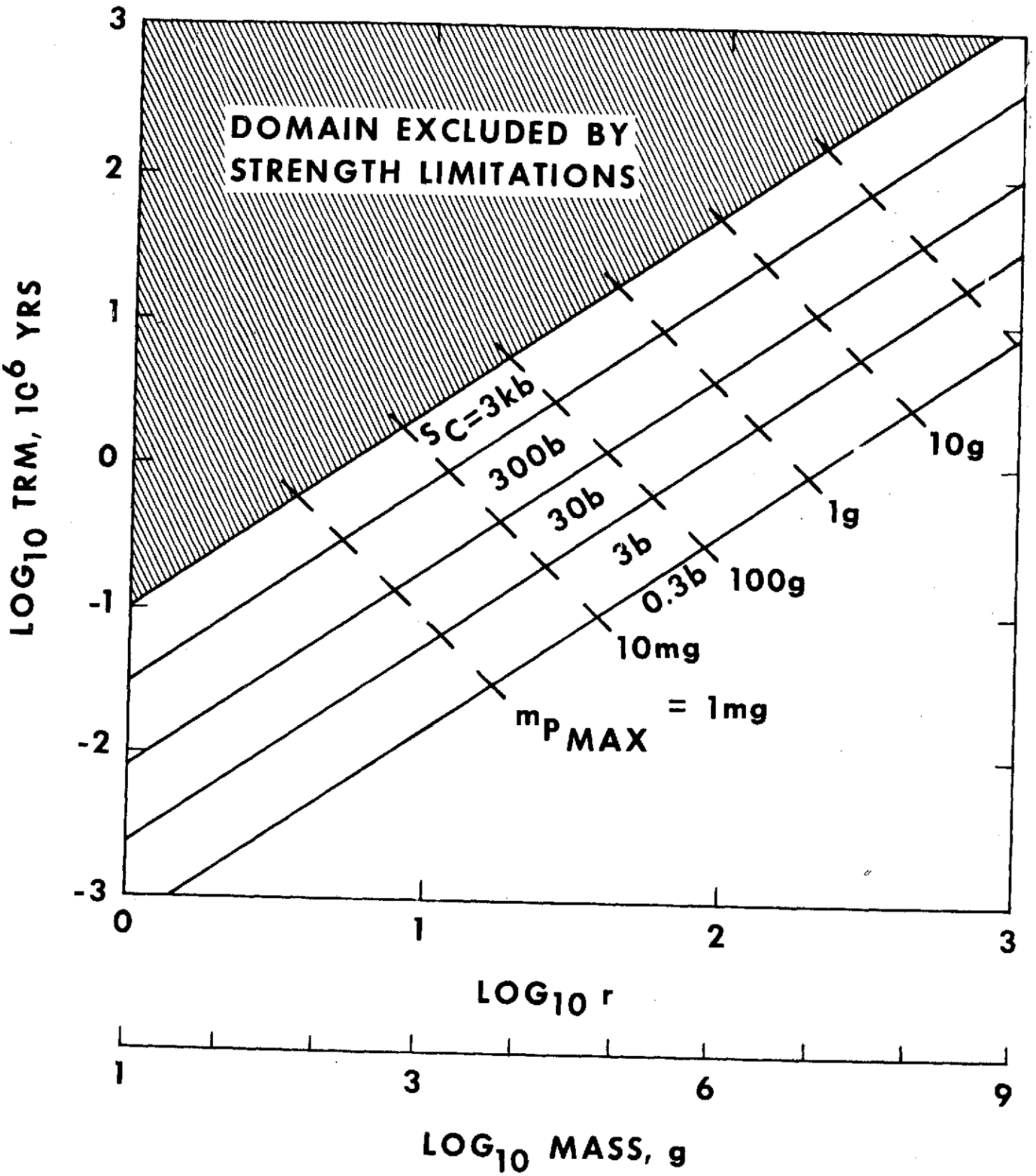
DOMAIN EXCLUDED BY
STRENGTH LIMITATIONS
s_C=3kb
300b
30b
3b
0.3b
10g
1g
100g
10mg
$m_{P_{MAX}}$ = 1mg
LOG_{10} TRM, $1C^6$ YRS
3
2
1
0
-1
-2
-3
0
1
2
3
LOG_{10} r
1
3
6
9
LOG_{10} MASS, g